# Manuscript Details

| | |
|---|---|
| **Manuscript number** | GEODER_2017_34 |
| **Title** | Quantitative characterization of soil micro-aggregates: new opportunities from sub-micron resolution synchrotron X-ray microtomography |
| **Article type** | Research Paper |


**Abstract**

Soil microaggragates are the fundamental building block, at the micron scale, of the highly hierarchical structure of soils, and can exert a significant control on the local biological metabolism and microbial community partitioning. In this study we propose an analysis protocol for the morphometric characterization of complete soil microaggregates based on sub-micron resolution synchrotron X-ray microtomography. A comprehensive characterization of the aggregate morphology is the first step towards a complete characterization of the soil microaggregates, when trying to correlate morphometric parameters with physical and/or biological properties, or when building models (e.g., effective diffusivity, microbial distribution, etc.). We demonstrate our characterization approach on two single microaggregate samples from dramatically different soil environments: one from Kansas, primarily composed by inorganic particles, and one from Barrow (Alaska) dominated by plant fragments. A series of state-of-the-art morphometric analysis techniques have been employed providing quantitative results highlighting specific differences of the two samples. The role of the microstructure in a scenario microbial population development has been discussed and it has been found that the Barrow microaggregate seems to be more favorable, from a purely geometrical point of view, as also confirmed by a simple model presented in this work. The potential of this approach, when coupled with chemical and biological analysis for a fully comprehensive characterization of soil aggregates in the larger picture of enhanced biological activity, is evident.



| | |
|---|---|
| **Keywords** | Synchrotron X-Ray microCT; Soil microaggregate; Quantitative image analysis; Modeling. |



| | |
|---|---|
| **Corresponding Author** | Marco Voltolini |
| **Corresponding Author's Institution** | Lawrence berkeley National Laboratory |
| **Order of Authors** | Marco Voltolini, Neslihan Taş, shi wang, Eoin Brodie, Jonathan Ajo-Franklin |
| **Suggested reviewers** | Marco Keiluweit, Francesco De Carlo, John Crawford, Mark Rivers, Hu Zhou |

## Submission Files Included in this PDF

**File Name [File Type]**

Geoderma_coverletter_voltolini.docx [Cover Letter]

ARef_geoderma.docx [Response to Reviewers]

Voltolini_soil_maggr_geoderma_revised.docx [Revised Manuscript with Changes Marked]

Highlights.docx [Highlights]

Graphical_abstract.tif [Graphical Abstract]

Voltolini_soil_maggr_geoderma_revised_nohighlightedch.docx [Manuscript File]

Fig_1.tif [Figure]

Fig_2.tif [Figure]

Fig_3.tif [Figure]

Fig_4.tif [Figure]

Fig_5.tif [Figure]

Fig_6.tif [Figure]

Fig_7.tif [Figure]

Fig_8.tif [Figure]

Fig_9.tif [Figure]

To view all the submission files, including those not included in the PDF, click on the manuscript title on your EVISE Homepage, then click 'Download zip file'.

Dear Editor,

please find the manuscript submitted for publication in “Geoderma” with the title:

***Quantitative characterization of soil micro-aggregates: new opportunities from sub-micron resolution synchrotron X-ray microtomography***

by
Marco Voltolini, Neslihan Taş, Shi Wang, Eoin L. Brodie, Jonathan B. Ajo-Franklin

With corresponding author:

*Marco Voltolini*
e-mail: mvoltolini@lbl.gov
Address: Lawrence Berkeley National Laboratory, #1 Cyclotron Rd, 94720 Berkeley, California, USA. Mailstop 74R316C
Phone: +1 510 486 4093

The manuscript submitted illustrates the analysis of two different (in origin, composition, and morphology) soil microaggregates via synchrotron X-ray microtomography. While this technique has been already employed in the past for similar purposes, there are many significant novel aspects in the present work:

1) Data quality: with the 325 nm per px of theoretical resolution of the reconstructed datasets, coupled with novel reconstruction techniques such as phase retrieval algorithms, the quality of the data is unprecedentedly high. This allows more precise analysis compared to most of the data present in literature.
2) Quantitative morphometric analysis completeness: no other soil dataset present in literature has been characterized in a quantitative fashion to this extent. This completeness helps with a better characterization, but also in finding the key morphological parameters and they relation with the sample properties.
3) Having measured (and analyzed) the *whole* soil microaggregate, and not a cropped volume as typically done, opened opportunities for novel analysis strategies, e.g. the calculation of the sample outer surface and the measurement of the openings of the microaggragate. A characterization of the interface with the outer world is of paramount important to better understand the dynamic equilibrium of the aggregate with the surrounding environment, and this characterization is not present in literature.
4) The points above can lead to a model aimed at calculating the pore space accessible to different classes of microorganisms (from a purely geometrical point of view). While simplified, such a model can potentially highlight (coupled with the analysis in #2) different physical properties (diffusion, microbial populations, etc.) in aggregates with different morphological characteristics.

Even if this work is mostly on the technical side, we find that the results can be of interest to the community of the soil scientists. The improved data collection/reconstruction procedure, coupled with the most advanced morphometric characterization, can provide the soil scientists novel analysis tools and procedures to better understand the complexity of soils; or to be coupled with local biological information; or to be used as a realistic

starting point for modeling. Also for this reason we plan to make the datasets (including surfaces, skeletons, etc.) available to the public on an online database, after publication, given its broad interest, difficulty of execution (a correct skeleton, a proper outer surface, etc. are not just a click on a software GUI, unfortunately), and general interest.
We hope you find the present work interesting and worth of publication in Geoderma, we have checked publications on this journal concerning X-ray microCT and we find this work could be a proper addition in that area, and could be of general interest to the scientist interested in better understanding the microstructure of soils at the nano- and micro- scale.

If suggestions for possible referees were welcome, I'd consider:

John W. Crawford
john.crawford@rothamsted.ac.uk
Rothamsted Research
West Common, Harpenden, Hertfordshire, AL5 2JQ

Marco Keiluweit
keiluweit@umass.edu
Stockbridge School of Agriculture
411 Paige Laboratory
University of Massachusetts
Amherst, MA 01003

Mark Rivers
rivers@cars.uchicago.edu
GSECARS, University of Chicago
Building 434A, Argonne National Laboratory
9700 South Cass Ave.
Argonne, IL 60439

Francesco De Carlo
decarlo@aps.anl.gov
Argonne National Laboratory
9700 S. Cass Ave
Building 438-B002

Sincerely

Marco Voltolini

Dear Editor,

Please find below the answers to the comments from the referee point by point (our answers in blue)

---

The authors present a method for the high-resolution scanning of microaggregates (<250 micrometers) using SXR-CT and associated calculation and display of summary metrics and networks derived from this scanning. The method is certainly of interest to the soil science community and the authors do a nice job of justifying their work. The manuscript is generally well written and was a pleasure to read. There are several points of clarification and organization, however, that I urge the authors to address as well as grammatical and cosmetic changes that should improve the flow and clarification of the manuscript.

I recommend moving the discussion of the sphere-normalized surface-to-area volume ratio in L649-658, the Minkowski functionals in L664-684, and the fractal dimension in L695-701 to the methods section as these describe the metrics used in the manuscript.

We understand the suggestion of moving the introduction of those analysis tools in a separate section, but we think that those paragraphs are belonging to the dedicated morphometric analysis section, where each technique is introduced and then the specific results shown. It keeps the flow of concepts more uniform and tidy, without the need of going back-and-forth mentally.

Sample choice -> Measurement -> Data optimization and cleaning -> Measurements on the data divided by type and their results -> Final Discussion.

The biggest limitation to the proposed method is a lack of discussion of error or uncertainty with the resulting metrics. For example, the statement on L1280-1282 that “it is clear that the microaggregate richer in organic matter (Barrow) is about twice as porous as the predominantly inorganic one (Kansas)” assumes that the two aggregates chosen represent the two environments from which the sample was taken. Can any conclusions really be made between two aggregates less than 250 micrometers in diameter separated by 3000 mi? What is the variability of the various resulting metrics determined from the scanning for each site? Although the authors insert a statement in L1294 that “…a statistically valid generalization from one small sample set is not possible…” they do not attempt to deal with this very real problem. Can the authors shed light on how many samples, for example, need to be taken to appropriately characterize the variability of the results? It seems to me that the smaller the unit of examination (which the SXR-CT enables) the more important the need for replication and an understanding of variability.

This is indeed a very important issue, but a comprehensive discussion about representativeness would require an effort beyond the scope of this work. As we claim, this is not about comparing two localities, but two microaggregates. “Kansas” and “Barrow” are intended as labels for the microaggregates, not for the localities.

Ideally, the only way to answer would be to measure a large amount of single microaggregates and calculate the heterogeneity among aggregates, for each morphometric analysis procedure. If we consider the single microaggregate as an object of the “microaggregate” class, a typical number of measurements would typically vary from hundreds to thousands objects (these are typical numbers for shape preferred orientation analysis, as in Voltolini et al., 2011 cited in the text). But the number of microaggregates needed for reaching statistical meaningfulness could also depend on the single parameters considered (e.g., the distribution of the porosity could be much sharper than the aspect-ratio). This is beyond the scope of this work, which is focused on finding the parameters that can better characterize differences in single microaggregates, not a comparison between “all” Kansas and Barrow microaggregates. We only wanted two markedly different (in texture/composition) aggregates to check which are the parameters that can better describe their difference (and their impact on some of the microaggregate physical properties). Actually, if the focus would be the comparisons of two locales, the best approach would likely be a multi-resolution one, where info at different scales and resolutions are combined, since a large number of measurements (and analyses!) on single microaggregates would require a huge and at present unrealistic amount of time and effort, which a multi-scale approach (where in low-resolution scans different classes of microaggregates *could* be identified and labeled) could -in theory- reduce.

We have added in the text some comments in the discussion section addressing this issue, as properly suggested by the reviewer.

There are multiple problems with punctuation in this manuscript especially with the use of commas. For instance, all uses of “e.g.” require an immediate subsequent comma (e.g., L130). Uses of a conjunctive adverb (e.g., “thus”) should be preceded and followed by commas where appropriate (e.g., L141).

Corrected

There are several times where the authors utilize the abbreviation “e.g.” outside of a parenthetical statement (e.g., L218). In these cases, the “e.g.” should be spelled out as “for example” with a subsequent comma.

Corrected for all the occurrences in the text

In multiple places, the authors have used a colon where a semicolon is actually appropriate (e.g., L218, 305, etc.). These colons should be changed throughout the manuscript where appropriate.

Corrected as suggested where needed.

Other detailed changes include:

L262 Change “scientists” to “scientist.” +

L305 Change “somehow” to “somewhat.” +

L313 Replace “techniques example on” with “of.” +

L344 The phrase “in the scenario of the origin of ‘hot spots’ in soils” is unclear. Please reword to clarify your use of the term “hot spots.” +

L361 Add “Biological Station” after “Konza Prairie.” +

L367 Change “amongst” to “among.” +

L382 Change “prior the” to “prior to the.” +

L384 Change “is” to “was.” +

L527 Change “int” to “into.” +

L610 Change “of” to “between” and “chosen” to “made.” Remove “the one.” +

L619 Replace “allowing us” with “the ability.” +

L622 Change “but smaller features, e.g. single clay minerals platelets, cannot be resolved” to “but without the ability to resolve (e.g., single clay mineral platelets).” +

L645 Make “Surface Area” lowercase. +

L649-651 Make “Sphere-Normalized Surface-to-Area Volume Ratio” lowercase. +

L666-676 Make “Integral Mean Curvature” lowercase. +

L680 Make “Characteristic” lowercase and remove “instead.” +

L695 Make “Fractal Dimension” lowercase. +

L732 Change “previously” to “in section 2.3.” Change “Local Thickness” to “LT” since the abbreviation is already defined in L546. +

L744 Add “of” after “modeling.” +

L807 Change “will be further discussed later” to “are discussed in section 4.” +

L826 Make “Connected Component Labeling” lowercase. +

L865-867 Change “While an approximation based” to “Although this approximation is based.” +

L867-869 The phrase “…such calculations allow hypotheses to be generated regarding what regions…” is awkward and unclear. Please reword. +

L1072 Add “sample” after “Kansas.” +

L1143 Make “Star Length Distribution” lowercase. Since many readers will likely be unfamiliar with this method, I recommend adding a brief sentence describing it in general. +

L1162 Make “Pole Figures” lowercase. +

L1180 Should “distribution” be changed to “density?” “Density” and “Distribution” are both correct and used in general texture analysis. In all my previous publications involving texture analysis I’ve used “Distribution” and I’d like to keep that definition for consistency. Interestingly enough, a similar issue exists for the Orientation Density/Distribution Function (ODF), where “distribution” seems to be slightly preferred. But they are interchangeable.

L1182-1184 What about values less than one? +

L1184 I’m unclear what the authors mean by “whole particle.” +

L1183 How is the shape of the particle elongated vertically shown in the figure? +

L1195 Change “constiturents” to “constituents.” +

L1203-1205 Change “Hints about the relationship of the PF’s with the sample” to “Relationships between PFs and the sample.” +

L1207 Change “PF’s” to “PFs.” +

L1209 Change “PF’s” to “PFs.” +

L1255 Change “such e.g. a Lattice” to “such as the Lattice.” +

L1576 Change “scientists” to “scientist.” +

L1636 Remove the comma after the second dash. +

The specific issues listed above marked with a “+” have been corrected as suggested.

Other minor changes have been done to improve the readability of the manuscript.

# *Quantitative characterization of soil micro-aggregates: new opportunities from sub-micron resolution synchrotron X-ray microtomography*

Marco Voltolini[1], Neslihan Taş[1], Shi Wang[1], Eoin L. Brodie[1,2], Jonathan B. Ajo-Franklin[1]

[1] Earth and Environmental Sciences, Lawrence Berkeley National Laboratory, Berkeley, CA 94720.

[2] Department of Environmental Science Policy and Management, University of California, Berkeley, CA 94720.

***Abstract***

Soil microaggragates are the fundamental building block, at the micron scale, of the highly hierarchical structure of soils, and can exert a significant control on the local biological metabolism and microbial community partitioning. In this study we propose an analysis protocol for the morphometric characterization of complete soil microaggregates based on sub-micron resolution synchrotron X-ray microtomography. A comprehensive characterization of the aggregate morphology is the first step towards a ~~comprehensive~~complete characterization of the soil microaggregates, when trying to correlate morphometric parameters with physical and/or biological properties, or when

building models (~~e.g.~~e.g., effective diffusivity, microbial distribution, etc.). We demonstrate our characterization approach on two single microaggregate samples from dramatically different soil environments: one from Kansas, primarily composed by inorganic particles, and one from Barrow (Alaska) dominated by plant fragments. A series of state-of-the-art morphometric analysis techniques have been employed providing quantitative results highlighting specific differences of the two samples. The role of the microstructure in a scenario microbial population development has been discussed and it has been found that the Barrow microaggregate seems to be more favorable, from a purely geometrical point of view, as also confirmed by a simple model presented in this work. The potential of this approach, when coupled with chemical and biological analysis for a fully comprehensive characterization of soil aggregates in the larger picture of enhanced biological activity, is evident.

*Keywords: Synchrotron X-Ray microCT; Soil microaggregate; Quantitative image analysis; Modeling.*

## *1. Introduction*

Soil is perhaps the ultimate "complex system", with physical, chemical and biological components interacting in a non-linear manner yet displaying clear properties of co-evolution and self-organization (Young and Crawford, 2004). The physical structure of soil acts in a deterministic manner to regulate the assembly and activity of soil biota, including microorganisms, and through their activity, soil biota continuously shape and

re-form both the macroscale and microscale structure of soil that in turn poses new constraints on biological activity. This pattern of co-evolution has led to the concept of soils being considered as 'extended composite phenotypes', (Phillips, 2009) where soils themselves "*are an expression of the cumulative impacts of the biosphere on surface processes*". As the fundamental units of soil, aggregates and their physical, chemical, and biological properties could be considered an extended soil phenotype.

The aggregation properties of soil constituents lead to a classification of aggregate forms, primarily based on size and basic physical properties (~~e.g.~~ e.g., stability in water, Six et al., 2000). Microaggregates, those less than 250 μm in diameter (Edwards and Bremner, 1967) are critical for the sequestration of carbon in soil (~~e.g.~~ e.g., Six et al., 2000, 2004, Vogel et al., 2014). Within microaggregates, pore structural properties that evolve during aggregate formation and stabilization result in organic matter being encapsulated within submicron pores (McCarthy et al., 2008) and, thus, protected from microbial decomposition due to kinetic and spatial constraints. Given its importance, the relationship between pore space geometry on the diversity and activity of soil microorganisms has been a topic of notable interest (reviewed in Or et al., 2007). Significant fractions of soil pore space can be inaccessible to soil bacteria (Chenu and Stotzky, 2002), and observations of bacteria confined within pore spaces are common (Foster et al., 1988), while predators such as protozoa can be isolated from their bacterial prey due to the interaction between pore geometry and the larger cell dimensions of protozoa (Vargas & Hattori, 1986, Wright et al., 1995).

Perhaps the strongest constraints on microbial metabolism within microaggregates are those of gas, moisture, and solute transport. Diffusive gas transport in particular is

limited by the aperture and connectivity of exterior pores to deeper environments as well as pore hydration state. In the near-surface, anoxic microenvironments can develop in the interior of microaggregates due to $O_2$ diffusion limitations as well as aerobic communities on aggregate surfaces. Due to the difficulties in measuring spatial concentrations gradients within microaggregates, many studies exploring these constraints focus on modeling approaches (Currie, 1962; Smith, 1980; Renault & Stengel. 1994; Ebrahimi & Or, 2015). Currie (1962) and Smith (1980) provide 1D continuum analytical models for such processes which are strongly dependent on an averaged $D_{eff}$, the effective gas diffusivity of the aggregate. Aggregate-specific $D_{eff}$ values are difficult to estimate, particularly for partial saturation states where capillary-bound water impacts gas transport. Ebrahimi and Or (2015) present a pore-resolved numerical model of gas and nutrient diffusion in microbially active aggregates and demonstrate that aerobic and anaerobic microenvironments quickly develop; such spatial gradients in turn drive community partitioning, particularly in wetter environments. A common limitation~~s~~ of all such studies is the absence of realistically parameterized pore geometries, particularly for microbially "remodeled" aggregates which are unlikely to have homogeneous network structures as shown in prior imaging studies (~~e.g.~~ e.g., Peth et~~.~~ al. 2008, Alba-Tercedor et~~.~~ al. 2015).

Given the importance of soil pore geometry and pore network connectivity for biodiversity and biogeochemical cycling, it is critical to develop quantitative measurement approaches to obtain soil aggregate microstructure at the relevant length scales (i.e. sub-micron). The microstructure of these fundamental soil building blocks will likely have a significant impact on the ability to host specific microorganisms~~;~~,~~:~~

~~e.g.~~ for example large pores with many small apertures can provide a safe environment for specific microorganism colonies to thrive. The direct correlation of microstructure and microorganism distribution is beyond the scope of this work, which focuses in on development of morphometric parameters and analysis strategies to obtain a comprehensive description of the microstructure of soil microaggregates. Our results do, however, provide insight into prior experimental studies examining the role of microaggregates in disrupting predation (Wright et ~~.~~al. 1995, Vargas and Hattori, 1986).

A first attempt at correlating Synchrotron X-Ray micro-Computed Tomography (SXR-µCT) data with microbial populations obtained via 16S rRNA pyrosequencing has been attempted in Bailey et al. (2013), where no clear correlation of microbial populations with microstructure has been found. While that work is valid, the lack of an advanced analysis of the SXR-µCT data (only proxies of pore size distributions and surface areas have been considered as descriptors for the microstructure) might have neglected important hints that could have been successful in finding an eventual correlation. In this context, we are offering an example of a state-of-the-art measurement and data analysis that can be used for a complete characterization of *whole* (in contrast with cropped subvolumes, as usually found in literature) soil microaggregates at the nanoscale, providing the soil scientist~~s~~ community a series of tools that can be used in future works where a comprehensive *quantitative* characterization of soil microaggregates is needed.

XR-CT (both using conventional and unconventional radiation sources, at different scales) has been successfully used for soil characterization in the past, given its ability to provide 3D volumes describing the structure soil samples. One of the main

advantages of this technique is its non-destructive nature, which allows the observation of undisturbed samples, such as roots in soils (Heerman et al., 1997; Mooney et al., 2013), macropores in large (~20 cm) soil cores (Pierret et al., 2002), and characterization of pore space in ~3 mm aggregates (Nunan et al., 2006;, Peth et al., 2008). More specific works, focusing on the characterization of the pore networks in soils, at different scales, can be found in Petrovic et al. (1982), and Anderson et al. (1990) where the main focus was the estimate of the density of the soil samples. At the mm scale, XR-CT has also been used to locate layering in soil samples as presented by Macedo et al. (1998). Other studies included porosity and flow properties in measured soils, as presented in Peyton et al. (1992), Heijs et al. (1995), Clausnitzer and Hopmans (2000). Fractal properties in soils have been studied although their calculation and practical implications have been somewhathow controversial. Examples can be found in: Perfect et al., (1992), McBratney (1993), Peyton et al., (1994), Anderson and McBratney (2005), Gimenez et al., (1997), Gibson et al. (2006).

In this work we present state-of-the-art data processing and morphometric analysis techniques example onof two different soil microaggregates (slightly smaller than 250 μm) to quantify microstructural attributes. The purpose is to show an analytical protocol that can be used to describe the microstructure of the soil microaggregates in a quantitative fashion, and to provide the scientific community (e.g.e.g., modelers) with datasets of *complete* microaggregate particles with sub-micron resolution to be used as a realistic starting point and/or validating dataset for synthetic soil models. To validate this approach, wWe have chosen two markedly different soil microaggregates, both in composition and texture, the first rich in inorganic material and the second rich in organic

material (plant fragments) to better monitor which parameters can describe those differences. This quantitative description of the soil microaggregates is fundamental for a complete study complementing the role of the soil microaggregates microstructure, chemical heterogeneities, and microorganism distributions in ~~the scenario of~~ the research about the origin and development ~~origin~~ of "hot spots" in soils, and to contribute to our understanding of the functional stability and spatial variability within soils in general.

## *2. Materials and Methods*

### *2.1 Sample choice and preparation*

Two distinct soils were selected for our study: one from the Konza Prairie Biological Station, Kansas, and a second from Barrow Experimental Observatory (BEO), Alaska. The two samples selected for this evaluation varied in bulk density, organic matter content, and mineralogy, among~~st~~ other parameters. Microaggregates were obtained via manual dissection under a microscope, where the sorting was based on size (200 to 250 µm diameter), and on the ability to remain coherent under mechanical stimulation. Preparation of the aggregates for analysis involved inserting the microaggregates into a thin walled 300 µm borosilicate glass capillary (Charles Supper); the capillary tubes were immediately sealed using hard wax to maintain the original humidity as much as possible. The capillary tube was used to assist sample mounting and to maintain sample integrity at proper moisture conditions. Sealing and acclimation (~1 hour) at the synchrotron

beamline experimental hutch prior to the experiment is fundamental to keep the soil aggregate at proper conditions and avoid motion artifacts due to variations in humidity during the scan. The very high resolution of the measurement makes the dataset prone to motion artifacts, so a nearly perfectly stable sample wais a necessity.

*2.2 SXR-μCT measurement and data reconstruction*

The SXR-μCT experiments were carried out at X-ray Imaging Beamline 8.3.2 (BL 8.3.2) at the Advanced Light Source (ALS) at the Lawrence Berkeley National Laboratory (LBNL). For the tomographic measurement, a 11 keV monochromatic beam was selected via a multilayer monochromator. The glass capillary containing the individual aggregates was mounted on a rotating stage, ~8 mm from the scintillator of the detector system; a short distance was selected to avoid strong phase-contrast effects due to free space propagation of the highly coherent XR beam. The detector system consisted of a LuAG 20 μm thick scintillator mounted in front of a 20×~~x~~ objective lens; the visible light signal obtained from the scintillator was recorded on a CCD camera (Optique Peter, Lentilly, France) obtaining a dataset with a resulting voxel size of 325 nm. 1800 projections were recorded for each sample over a 180° rotation, and the exposure time was 1 second per projection.

Before reconstruction of tomographic 2D slices, a single-distance phase retrieval algorithm was applied to the projection datasets. Phase-retrieval is beneficial in this kind of datasets since it improves the contrast between the different phases and makes the phase-contrast artifacts less pronounced, both these characteristics are of great help with

the segmentation via thresholding process. After a conventional flat-field correction of the single projection, we applied the Paganin single-distance phase retrieval algorithm (Paganin et al, 2002) as implemented in the ImageJ plugin ANKAPhase (Weitkamp et al., 2011), which proved to be effective (~~e.g.~~e.g., ~~Voltolini~~ Arzilli et al., 201~~57~~) with datasets collected in the near-field Fresnel diffraction region (Bronnkov, 2002). After phase-retrieval the slices were reconstructed with a conventional filtered back-projection algorithm (Kak and Slaney, 1987).

Once the stacks of slices were reconstructed, the datasets were manually cropped to isolate the soil microaggregate, separating it from the glass capillary, to obtain an 8 bit grayscale volume used as a starting point for subsequent analysis. The volume rendering of the two particles, whole and with a virtual vertical cut to show the internal structure, are shown in Figure 1. It is immediately possible to qualitatively appreciate the microstructural differences and identify in the "Barrow" microaggregate a large amount of material originating from plant debris, visible as a cellular texture with large interior pores (right panel). In contrast, the microaggregate obtained from the Kansas prairie site (left panel) appears to be an aggregate of mineral particles with smaller interior pore spaces, displaying a more interstitial type of pore space.

*2.3 Data treatment and separation*

To allow analysis of pore-space morphologies, the first step in our analytical approach is segmentation, aimed at separating the phases of interest into binary volumes. A simple manual thresholding procedure was possible due to the strong contrast between the solid

and voids voxels in the samples obtained after the phase retrieval procedure. However, the analysis of microaggregates requires a deviation from classical approaches for segmentation commonly applied to XR-CT datasets. In most situations, the image volume is cropped and only a subsection of the system is segmented and analyzed. In our case we wanted to capture the entire particle and determine the properties of the aggregate exterior surface. This boundary forms the interface between the aggregate and the outside world and is key to imposing boundary conditions when looking for interactions of the outside with the microaggregate pore space, ~~e.g.~~for example ~~for~~ in gas transport modeling, predation, etc. This approach comes with a challenge, mainly the problem of separating the air outside the microaggregate from the air in the voids inside the sample despite the fact that the phases are continuous. This cannot be done ~~with~~ via thresholding procedures, since the air inside and outside the sample has of course the same XR attenuation values (translated into the same grayscale value, in the tomographic dataset), thus the necessity of morphology-based methods.

We have developed an iterative procedure using the Fiji software framework (Schindelin et al., 2012) that allows the calculation of such an external surface and provides a separation of the pore space from the air outside the sample. This procedure can produce results similar in concept to the snake-based "active contour" segmentation algorithms used in the medical imaging field (~~e.g.~~e.g., Yushkevich et al., 2006). The procedure we applied ~~also functions~~works well in 3D and can be applied to systems where large objects need to be extracted and segmented. The procedure consists of a series of operations involving local thickness (LT) analysis of the voids using the plugin described in Dougherty and Kunzelmann (2007). LT analysis is used to obtain a first,

rough, outer surface and a closing procedure is used to close the smaller outer pores. 3D void filling is then used to fill the largest internal voids, and finally masking is utilized to preserve the small features that are commonly erased by the morphological operators such as eroding and dilating processes. The filled soil aggregate particle obtained is then used to obtain a "sample surface" again through morphological operators of the binary erosion/dilation class coupled with Boolean operations. This outer surface obtained with the procedure described above is shown in Figure 2 rendered in red and superimposed on a rendering of the Barrow sample. The virtual cuts reveal how the surface calculation effectively "wraps" the aggregate exterior without penetrating into the interior pore spaces, thus providing information on the interface between the aggregate and the surrounding environment. The procedure of calculating a surface separating the pore space from the outer air is the starting point for subsequent analyses on the two datasets.

## ***Results***

### *3.1 Morphometric analysis: Basic analysis*

The procedure described above generates two base binary volumes for the morphometric analysis: a volume for inner voids (the pore space) and a volume of the solid phase. This allows a variety of analytical techniques to be carried out in order to obtain quantitative information describing the two different phases. We stress that all the morphometric analysis needs to be considered with the actual resolution of the measurement in mind;

some values (such as surface area values) are very sensitive to image resolution and the value listed must be read with this intrinsic limitation in mind. For SXR-µCT anaylsis, a compromise betweenof field of view and resolution needs to be chosenmade;: we have chosen the one the setup with the abilityallowing us to image thea whole soil microaggregate with the highest resolution possible.; With the chosen setup the resolution was very high, especially when compared to similar measurements presented in literature, but still without the ability to resolve thebut smallestr features, (e.g.e.g., single clay minerals platelets), cannot be resolved. We present a comparison of a range of classical morphometric metrics applied to our two samples, including porosity, surface area, sphere-normalized surface-area-to-volume-ratio, Minkowski functionals, and fractal dimension metrics; such metrics provide a first step in grouping aggregate properties.

The first analysis carried out was to calculate the basic properties of the aggregates, such as their volumes and porosities. In Table 1, a summary of the morphometric analyses carried out on the two samples is listed. From the volumetric analysis, we can see how the Barrow sample is ~22% larger in volume than the Kansas one. The cellular texture and interior pores seen in the Barrow sample results in a high porosity (81%) while the Kansas aggregate has a porosity more typical of granular composites (43%). The sSurface aArea (SA) calculation also shows a higher value for the Barrow sample but the impact of sample size makes such a non-normalized SA problematic to interpret. To overcome this problem a sSphere-nNormalized sSurface-to-aArea vVolume rRatio (SNSVR) was calculated with SNSVR defined as $SA_{obj}/SA_{sph}$. $SA_{obj}$ is the object surface area, and $SA_{sph}$ is the surface area of a sphere with the same volume of the object. The farther the object surface is from a spherical surface, the higher

the SNSVR value (1 being the value for a perfect sphere). After this correction, the Barrow sample still shows a larger area available per volume units, but both the microaggregate particles display values related to a markedly complex surface.

The Minkowski functionals (see ~~e.g.~~e.g., Ohser and Muecklich, 2000) can be used as topological descriptors of a binarized volume. More specifically the i~~I~~ntegral m~~M~~ean c~~C~~urvature (IMC) (Russ and DeHoff, 2012) is a value related to the concavity/convexity (depending on the sign of the IMC) of the surfaces present in the sample. The Euler c~~C~~haracteristic (EC) (Odgaard and Gundersen, 1996) is ~~instead~~ a value related to the connectivity of the objects in the volume: positive values mean isolated objects, while connected networks generally display negative values. The values measured for the IMC of the framework of solids and the EC of the pore space highlight a highly connected network dominated by concave shapes of the solid framework, with the Barrow sample being slightly more interconnected and with a slightly weaker dominance of convex surfaces.

Another frequently used parameter for texture analysis is the f~~F~~ractal d~~D~~imension (FD), which has been applied to the solids in the aggregate, providing an index of self-similarity of the microstructural features at different scales. The FD has been calculated using the box-counting method (Liebovitch and Toth, 1989) and values obtained show that the Barrow aggregate (FD = 2.401) is slightly more self-similar than Kansas sample (FD = 2.353). Both values are relatively low (for volume data $2 \leq FD \leq 3$) highlighting moderate fractal properties, at the considered resolution and sample size. Prior studies examining the fractal dimension of micro-aggregates using destructive mass/radius analysis have yielded slightly higher values (FD = 2.75 to 2.93, Young & Crawford,

1991), the differences in sample origin and measurement approach make comparisons challenging.

*3.2 Local thickness (LT) analysis*

As discussed ~~previously~~in section 2.3, ~~Local Thickness (~~LT~~)~~ analysis is an extremely useful approach for porous material characterization borrowed from the bone scientist~~s~~ community, where it is generally used for the analysis of cancellous bone, measuring parameters such as the "trabecular thickness" and "trabecular separation" (Parfitt et al., 1987; Simmons and Hipp, 1997; Accardo et al., 2005). The same algorithm has been later adopted in different contexts ~~e.g.~~for example as part of multiphase flow modeling approaches by Silin et ~~.~~al. (2010) under the name "maximum inscribed spheres" and is finding increased use in modeling of geologic samples. The term "local thickness" for a voxel is used to mean the diameter of the maximum inscribed sphere in the structure that contains the voxel. In Table 1., where the LT results are summarized, we use more generic terms, where "structure separation" is the LT analysis calculated on the pore space volume, while with "structure thickness" we mean the LT analysis carried out on the solid framework. The analysis has been performed using the Fiji plugin from Dougherty and Kunzelmann (2007), and graphical results are shown in Figure 3 for both the migroaggregates.

In Figure 3 a vertically cut rendering is superimposed with the LT-labeled volume of the pore space, and a volume rendering of the cut LT volume itself. The image clearly displays the thickness variations of the pore space within the volume, with the Kansas

sample showing interstitial voids created by the aggregation of the silt particles, while in Barrow the larger, smoother, voids due to the presence the plant fragments and their cellular structures are evident. A larger variation of LT values is also immediately observable from the renderings in figure. A quantification of the LT analysis was performed and the results are presented again in Table 1. The mean of the structure separation (mean LT of the pore space) is larger in the Barrow sample, but also the standard deviation is significantly larger and the maximum LT value of voids is present in the Barrow sample as well, this again because of the presence of the plant fragments with large voids surrounded by small ones. This variability is recognizable when looking at more detailed data than the one summarized in the Table 1. In Figure 4 we show a plot of the LT values distribution in the pore space for both Kansas and barrow. The higher variability suggested by the summarizing values here becomes even more evident with the two distributions being markedly different, with values of higher LT values being more frequent in the Barrow sample. The smallest LT values are also more frequent in the Barrow sample, while the small LT values are generally more frequent in the Kansas microaggregate, showing a sharper LT distribution curve. This feature and its implications ~~will be~~ are discussed in section 4~~further discussed later~~.

Concerning the structure LT analysis ("structure thickness") values for Barrow are generally slightly larger, with a much larger standard deviation value and especially a larger maximum. This because in the Barrow sample a ~50 μm large single mineral particle is present (top of the sample).

*3.3 Geometrical accessibility analysis*

The concept of LT, combined with the outer surface calculated via the procedure described above, and the cConnected cComponent lLabeling (CCL, see e.g.e.g., Hu et al. 2005) can be used to calculate the parts of the sample accessible from the outside by objects with different sizes. This class of analysis has obvious applications as a simple model able to provide insights about pore-size constrained microbial colonization of aggregates, as well as the spatial limits of predation by larger organisms. The procedure is straightforward: a threshold value (corresponding to the size of the structuring element -spherical- considered for accessibility) is applied to the LT volume. A 5 voxel thick outer surface is added to the volume and a CCL procedure is initiated starting from the outer surface;: this will find all the parts of the sample accessible from the outside. The outer surface is then removed using a masking procedure with the pore space binary volume. The volume left is the pore space geometrically accessible from the outside by a spherical element with the value corresponding to the threshold value used.

This procedure can be used to detect the parts of the pore space theoretically accessible to microorganisms of known size, using only geometric parameters. This isolates the volumes of the samples accessible by the different structuring elements form the outside, along pathways with throats larger than the structuring element. Although this approximation is basedWhile an approximation based solely on geometry, such calculations allow to obtain some information about which parts of the sample could be accessible to different classes of microorganisms, segmented by their characteristic size. hypotheses to be generated regarding what regions of the aggregate are accessible to different classes of microorganisms. Bearing in mind the resolution of the measurements,

we considered three different classes of microorganisms based on their size: 0.65 μm for average microbial cells, 2 μm for large microbes, and 10 μm for protozoa. Aggregate microarchitecture can be expected to influence the distribution and activity of microorganisms, for example microaggregates possessing large internal chambers with entrances small enough to selectively exclude larger competitors and/or predators would represent potential activity hotspots and refuges for select portions of the community. Results of the analysis are summarized again in Table 1. From this set of calculations, it is possible to see that both microaggregate samples are close to totally accessible to objects .65 μm large, while 2 μm structuring elements can still enter the majority of the pore-space in both the Barrow (86%) and Kansas (76%) samples. The largest (10 μm) structuring element, the size of small protozoa, cannot enter any of the pore space of the Kansas, inorganic-rich, microaggregate, while a small part of the sample (3%) is accessible in the Barrow one.

The potentially accessible parts of the pore space are displayed, superimposed to the 8bit volume rendering for all the particles in Figure 5. In this figure it is possible to observe the parts of the sample accessible to microbes of different sizes; for example the top lobe of the Kansas sample can be fully colonized by .65 μm microorganisms but has limited pore-space available to 2 μm microbes. Neither aggregate, with the exception of a single large pore in the Barrow sample, has a pores/throats system of sufficient size to accommodate 10 μm microorganisms, suggesting that both microaggregates could provide protection to internal communities from predation by protozoa. Previous microcosm studies have demonstrated that aggregate microstructure protects microbial communities from such predation (~~e.g.~~e.g., Vargas and Hattori, 1986, Wright et ~~.~~al. 1995)

but prior studies could not characterize the internal aggregate structure which confers this effect.

*3.4 Skeleton analysis*

Another important descriptor of pore network topology is the pore space skeleton. A skeleton is a 1D topological descriptor of the 3D pore space which captures network connectivity in a simplified form, suitable for discrete models of flow and transport. In this study we used the "thinning" algorithm to efficiently compute the medial axes of both aggregate pore spaces (Lee et al., 1994; Lindquist et al., 1996; Palágyi and Kuba, 1999). The skeleton of the pore space of the connected network was calculated and the skeleton voxels were also labeled to identify branches, joints and end points in the framework.

The results of the skeleton analysis are summarized in Table 2. The network statistics indicates that the Barrow sample has the greater pore network complexity; this sample displays a significantly larger number of branches and junctions while the number of end points and the average branch length are very similar. This feature highlights a similar, basic, accessibility from the outside to two networks markedly different in complexity. This topic will be further analyzed and discussed, when another concept of "accessibility", based on the analysis of the size of the openings of the microaggregates facing the outside will be introduced. In Figure 4 a frequency distribution plot of the branch lengths in the two microaggregates is shown: the Barrow sample displays a wider distribution, with a larger number of the smallest and larger branch lengths, while the

Kansas sample has a larger amount of the smaller (but not the smallest) branches. This, again, highlights the differences of the two pore network topologies, with the Barrow being the more complex.

The renderings of the two samples with the calculated thinning skeletons, labeled with respect to the LT value of each voxel to introduce pore diameter information in the skeleton, are shown in Figure 6. From the colors of the skeleton it is possible to see how in the Barrow sample the blue colors (extremely small values of LT) and the hotter colors (higher values of LT) are more frequent than in the Kansas sample, where small and moderately small (blue and greens) values are visibly more frequent. This is in accordance with the LT analysis discussed previously.

The network renderings also provide a qualitative representation of the differences in skeleton architecture between the two samples; the Kansas sample exhibits an interstitial skeleton, typical of the pore space generated from granular materials. In contrast, the Barrow sample shows more complicated structures, including components with many short branches and small LT values as well as parts with single long branches following the medial axes of the largest structures. These features appear to be generated by the interconnected cellular texture of the plant fragments incorporated into the aggregate.

*3.5 The interface to the outer world: openings analysis*

The outer surface of the aggregate is a critical interface linking it to the exterior environment, mediating gas and solute transport as well as microbial colonization. A key

numerical task is, thus, extracting the apertures which exist on the aggregate exterior; these components are the required boundary condition for pore-scale modeling of diffusion and reaction within the single microaggregate system. As discussed in previous sections, our processing flow has already extracted (a) the exterior bounding surface and (b) the skeleton and LT map for the aggregate pore space. By selecting the skeleton end-points which terminate within close proximity (5 voxel lengths) of the outer surface and then labeling them with the LT thickness we can generate a map of aggregate openings with the appropriate dimensions. The lower panel of figure 4 shows a histogram of the size of open pores on the aggregate surface for both samples considered. As can be seen, the slopes of the opening size distribution curves are markedly different, being the Barrow one steeper, highlighting a higher amount of small apertures, and a higher small-to-large apertures ratio. This is again a difference due to the Kansas being an aggregate of particles with an interstitial kind of pore space, while the Barrow is made of mainly small plant fragments with ~~either~~ very small openings with a the few extremely large ones, where the biggest sects of the plant structure are broken and exposed to the surface. This results in the markedly different distribution of the openings.

Figure 7 provides a more graphical representation of the opening calculations showing grayscale volume renderings of the two microaggregates with opening pores marked in color. The paired figures show the same openings superimposed to~~on~~ the internal network structure (the skeleton in white). As can be seen, both samples are dominated by small exterior pores with the Barrow sample having smaller opening dimensions, indicated by the cooler colors (blue). The large exterior pores (orange/red) are relatively rare features on both aggregate surfaces.

*3.6 Anisotropy analysis*

Soil microaggregates can be formed by different components with varying shapes including rounded mineral particles, clay platelets, and fibrous/cellular organic materials as well as bioproducts. The shape of these constituent materials can control the shape of the microaggregate and the presence of anisotropic components can influence soil aggregate properties (~~e.g.~~e.g., Emerson, 1959). Considering that existing continuum models of gas diffusion in aggregates assume isotropic effective diffusivities, detection of strong pore-space anisotropy is a useful tool for evaluating the applicability of such models.

Fabric anisotropy can be measured directly from high quality tomographic datasets. One such approach is described in Voltolini et al. (2011), however it requires the separation of each single object in the dataset, a difficult constraint for aggregate characterization. When interior object separation is not possible, different approaches can be used. The most widely utilized technique is the m~~M~~ean i~~I~~ntercept l~~L~~ength (MIL) method (Withehouse, 1974), but this shows some limitations since it ideally requires spherical cropping and is prone to artifacts in datasets with objects described by small numbers of voxels. To minimize these issues we decided to use the s~~S~~tar l~~L~~ength d~~D~~istribution (SLD) method (Odgaard et al., 1997), which measures the mean object lengths for all orientations, using the implementation present in Quant3D (Ketcham and Ryan, 2004) for the first calculation, ~~then~~ finally a series of Matlab® scripts based on the

MTEX toolbox (Bachmann et al., 2010) were used for data handling, corrections, normalization and plotting.

To study the anisotropy of the two microaggregates we applied the SLD method to the solids and on the filled shape of the whole microaggregates. The former provides the quantification of the anisotropy of the internal migroaggregate structure (solids), while the latter describes the anisotropy of the shape of the microaggregate itself. A comparison of the two pPole fFigures (PFs) obtained from this analysis highlights any relationship of the microstructure with the shape of the microaggregate. In Figure 8 the PFs describing the Kansas and Barrow microaggregates for the solids and the whole microaggregates are plotted. In the Kansas sample (top) it can be seen that the structure is made by isotropic/randomly oriented components, since the PF displays values extremely close to one along all directions. Values in PFs are in multiples of random distribution (m.r.d.), where 1 is the value of a perfectly isotropic object and higher values towards $+\infty$ imply progressively stronger anisotropy. The orientation space with values <1 imply an orientation density smaller than a random (i.e. isotropic, uniform) distribution, and in addition to the maximum value, the minimum value in the PFs is an important parameter as well, representing the percentage of objects in the sample that can build a random distribution, thus giving additional information about the sharpness of the texture. The PF for the Kansas whole microparticle aggregate denotes that some anisotropy is present;: this is clearly visible from the renderings where the shape of the particle is elongated vertically and slightly flat, similarly to a 3-axes ellipsoid. This result shows that even if the microaggregate particle is elongated, there is no internal anisotropy present, in its

components. This result is in line with the qualitative observation of the microaggregate constituents, where many rounded silt particles are recognizable.

The Barrow microaggregate is different; the PF of the whole particle suggests a slightly platy morphology, but the PF of the microstructure of the solids clearly shows a more fiber-like texture with the elongation axis in the platelet plane. The texture is weak (max at 1.25 m.r.d.), but anisotropy is clearly present. Relationships between PFs and the sample can be seen at the bottom of Figure 8 where the renderings of the soil microaggregates, with the same orientation as the PF's are displayed. The virtual cut plane of the aggregates corresponds to the plane of the PF's as well. This analysis confirms that an accurate quantification of the anisotropy in single soil microaggregates is achievable using the methods described above.

***Discussion***

Two soil microaggregates of different origins and internal structures have been analyzed via sub-micron resolution SXR-µCT. A variety of techniques to analyze different microstructural parameters have been applied to provide a description of the different features of the aggregate microarchitecture in a descriptive fashion. This class of approaches are increasingly used in analysis of soil systems (e.g.e.g., De Gryze et al., 2006; Peth et al., 2008a,b; Zhou et al., 2013; Ma et al., 2015; Peth et al., 2015). The potential flexibility of the resolution/FOV ratio, with both conventional and unconventional X-ray sources, allows scans within a large range of scales (Sleutel et al.,

2008). Synchrotron radiation, given its high flux, monochromaticity, and spatial coherence, has been recognized as a very important tool for the soil scientist since the first 3D imaging beamlines were developed (Spanne et al., 1994). Microtomographic data are also used for modeling more complex physical properties of soils and rocks, such ase~~.g. a~~ the Lattice Boltzmann approach for evaluating permeability (Menon et al., 2011; Khan et al., 2012) or direct numerical simulations of pore-scale reactive chemistry (Molins et al. 2012).

In this work we focus mainly on the geometrical differences of single microaggregates and exploit the high flux and resolution of BL 8.3.2 to provide a more detailed structural description. The new tools make it possible to develop the analysis of the entirety of microaggregates at sub-micron resolution, overcoming the need to crop subvolumes. This is of great importance since we were able to study the interface of the single microaggregates with the external world, whereas cropped volumes would make this kind of study impossible, and would not provide correct boundary conditions when used for modeling.

The size of the two microaggregate studied is similar. From the analysis of the internal porosity, it is clear that the microaggregate richer in organic matter (Barrow) is about twice as porous as the predominantly inorganic one (Kansas). This increased porosity appears to be the result of large pores with a cellular texture, as visible in Figure 2b. While a statistically valid generalization from our small sample set is ~~-~~not possible, the results from the Barrow aggregate suggest that detrital plant matter has an important role in controlling internal porosity. Prior studies of microaggregate structure have noted that formation often initiates around a “core” of plant debris (Oades and Waters 1991,

Golchin et al. 1994); our results suggest that this core material may also provide a unique structural environment for microbial activity distinct from microaggregates which are primarily granular in texture. It is important to remark that in this work we are only comparing two aggregates with different texture and composition to find the morphometric parameters that would better describe those differences, and the links of those parameters with specific properties of the aggregate; we are not comparing two specific environments. The latter task would require a much larger number of samples, and likely a different approach, combining multi-resolution measurements, where the large FOV would be used to identify the different type/classes of microaggregates present in each locale (and quantify their distribution), while the high resolution would target the specific single microaggregates (as shown in this work), representative for each class, to fully characterize them. Such an approach would likely allow reaching an acceptable statistical meaningfulness for each site, as needed to take into account some of the intra-site variability of microaggregates, but without measuring an unrealistically high number of single microaggregates and run a full analysis on all of them.

The iInternal aggregate surface area is another important parameter due to both its role in reaction kinetics as well as a microbial growth substrate. Concerning the surface area of the two microaggregates, the Barrow sample shows a larger surface area with a slightly higher complexity than the Kansas sample. This is likely due to the rough surface present in the Kansas sample, composed mainly of poorly sorted silt/clay particles, and the smoother surfaces present in the Barrow sample. However, the complexity of the pores space in the Barrow sample ultimately generates a higher surface area per volume.

The Minkowski functionals, as expected, describe a complex structure with a tightly interconnected pore space. This is also confirmed by the skeleton analysis, highlighting again the extensive complexity of the soil microaggregates at this scale. The fractal analysis shows a moderate fractal behavior for both the microaggregates, with no significant differences between the inorganic- and organic- based particles. Independent of use as a complexity measure, the fractal dimension of aggregates has been linked to measures of erodability in past studies (~~e.g.~~e.g., Ahmadi et al. 2011), hence it may such measurements may provide insight to microaggregate evolution over time.

The LT analysis discussed previously provides detailed information on pore space statistics across the aggregate; the distribution of voxel LT values provides useful statistical constraints including the aperture variance, a key parameter in stochastic network models of soil structure which is often guessed at. The LT distribution in the Kansas sample is clearly sharper than the Barrow aggregate, which exhibits a higher variance in pore sizes and apertures. This statistical difference is due to the plant fragments: the large voids present in these structures, coupled with small voids generated by clay particle aggregation, generated a broader distribution of pores. These observations suggest that the Barrow microaggregate might provide a better host for microbial activity due to the combination of a large internal porosity and a broad size distribution of internal microenvironments.

The novel strategy for soil particles analysis presented also allows the calculation of pore space accessibility metrics for single aggregates, potentially a key control on protection of aggregate microbial communities from predation by larger organisms (~~e.g.~~e.g., protozoa). It is worth remarking that this is a theoretical accessibility based

purely on the geometry of the pore space: ~~characteristics~~ features such as characteristic microorganism shape, biological needs, reproduction rates, etc. are not considered. The resulting accessibility metrics assume a rigid spherical body to determine the ideal potential access. We have chosen three different sizes, compatible with characteristic organism sizes and image resolution. First we have performed the accessibility analysis for objects .65 μm large, a typical mid-size bacterial cell. The theoretical accessibility for a virtual microorganism of this size from outside the sample is very large: 95% for the Kansas sample and 98% for the Barrow aggregate. This is not surprising since this value is close to the resolution of the measurement and the pore space is strongly interconnected. More interesting is the accessibility for objects with the size comparable to large bacteria strains: 2 μm. The differences here are more marked since some parts of the Kansas sample, more complex and with small, not well connected, pores are present and therefore they are non-accessible to the 2 μm virtual bacteria. In the Barrow sample the accessibility is still very high (86%, compared with the 76% of Kansas), this is due to the fact that the size of the object is still smaller than the size of a significant number of openings on the surface and because of the very high connectivity (and throat sizes) of the pore space, allowing the objects to move rather freely once entered the microaggregate pore space.

As a last test, we considered objects 10 μm large: this is the size of small protozoa, an active bacterial predator. Prior experimental studies (Wright et ~~.~~al. 1995) have utilized even larger protozoa with mean sizes in the 20-30 μm range (*C. steinii)* to study the protective nature of aggregates. A microaggregate largely accessible to protozoa would be potentially unsafe for the internal microbial community. In the two

microaggregates examined, the virtual protozoa cannot enter any pore space in the Kansas sample, and can only enter a small single portion of the pore space in the Barrow one, highlighting how these microaggregates can in theory provide a protective environment for bacterial communities. Our imaging study is largely consistent with prior experiments documenting this phenomenon (Vargas and Hattori, 1986, Wright et al. 1995). Given the protective role of microaggregates and the availability of a diverse set of associated microenvironments (Ranjard and Richaume, 2001), the role of aggregate pore morphology in controlling community structure might provide a promising path towards understanding the biogeochemical response of such systems (Remenant et al. 2009).

In addition to bulk accessibility metrics, we quantified the aperture dimensions of the outer surface of each aggregate sample, a metric useful in defining outer boundary conditions and flux limitations for gas transport. In the Kansas sample the exterior aperture sizes are generally larger than the Barrow sample as can be seen in the color map used in Figure 7. The Barrow sample does however have a small number of large open exterior pores generated by open tubular structures present in the detrital plant components. This analysis provides a quantitative approach to estimating the unoccluded surface/total volume ratio for the aggregate, a parameter required when modeling oxygen diffusion and consumption in aggregated soils (~~e.g.~~e.g., Renault and Stengel, 1994).

The analysis of anisotropy revealed that the Kansas aggregate is effectively isotropic in terms of microstructure despite an elongated shape. In contrast, the Barrow aggregate was anisotropic on the pore scale due to the presence of aligned pores in the detrital plant fragment. While we did not numerically compute effective diffusivity

coefficients for the two aggregate samples, the lower isotropy index for the Barrow sample (0.763) suggest that preferential diffusion along the axis of the aligned pores could significantly impact gas and solute transport.

Figure 9 provides a graphical summary of the analysis suite displayed for a thin (~20 μm) horizontal slice in each aggregate. Each image shows the typical characteristics discussed in this section and it is possible to better understand the differences in LT, skeleton and openings in the two microaggregates. In Figure 9a the 8bit rendering of the solids is superimposed with the LT volume: the differences in porosity and pore size distributions are immediately visible, as in Figure 9b (LT volume alone). In Figure 9c the 8bit volume is superimposed with the skeleton (labeled with the LT values) and the openings (labeled with a color corresponding to their diameter). It is possible to appreciate how well the skeleton fits the pore space and the role of the bigger chambers due to the presence of the plant fragments in the Barrow microaggregate. In Figure 9d the 8-bit volume is removed to highlight the features of the skeletons and of the openings: we see a more complex pattern of the skeleton in the barrow samples with shorter and smaller branching linking the outside of the particle with the pore space, while the Kansas particle displays classic interstitial pore space features in both the skeleton and the openings.

A significant potential use of the detailed structural analysis presented is for the direct numerical modeling of pore-scale biogeochemical processes in microaggregates. The recent study of Ebrahimi and Or (2015) presents an elegant network modeling approach capable of capturing the boundary of aerobic activity and community partitioning within a single aggregate. The network architecture used in the modeling,

however, was a theoretical regular framework generated to match capillary pressure/matric potential data on an aggregate collection and did not contain the detail present in our direct imaging study. We believe that high quality SXR-µCT can fill an important gap in such modeling studies by providing an appropriate network, aperture distribution, and set of boundary conditions to realistically capture biogeochemical processes at the aggregate scale. This interaction between experimentalists providing the modelers realistic starting points and validation datasets is bound to become more and more important in many fields. The new direction of building online experimental data repositories (~~e.g.~~e.g., https://www.digitalrocksportal.org/) will also have an increasingly important role in connecting experimental and modeling groups, including of course the soil scientist~~s~~ community.

***Conclusions***

SXR-µCT measurements on single soil microaggregates, coupled with advanced analysis techniques have significant potential to improve the characterization of this unique microbial environment. The suite of tools we present may aid future studies seeking to correlate aggregate microstructure with microbial community structure and function. In this study two markedly different microaggregates have been analyzed and the results show how soil microstructures can be quantified and potentially linked back to biological processes. Prior work has demonstrated a direct impact for different processes such as the protection from predators (Griffiths and Young, 1994; Young and Ritz, 1998), the

distribution of nutrients (Chenu et al., 2001), or for environmental issues such as local variations in heavy metal concentrations (Ranjard et al., 2000).

In the two samples we have shown the Kansas microaggregate, mostly inorganic in nature, displays a typical interstitial pore space, created by the aggregation of rounded mineral particles and aggregates. A more complex microstructure is present in the Barrow microaggregate, with a strong organic component, discernible also from the XR attenuation values, due to the high percentage of plant fragments. This microaggregate shows a significantly larger amount of pore space potentially available to bacteria, and this pore space is accessible only to small- to medium- sized microorganisms. Following the geometrical concept alone the Barrow microaggregate provides a better environment for the potential development of bacteria colonies, providing a larger and well protected space to the microorganisms.

The quantitative microstructural characterization -aim of the present work-~~,~~ albeit fundamental, is only a single ~~factor~~element for a truly complete characterization of soil microaggregates. The distribution of the chemical compounds needed for the development of the microorganisms, and of microorganisms themselves, in the microaggregates also play a key role and a comprehensive study about the role of microaggregates in the development of spots of highly increased biological activity in soils. Future improvements in X-ray imaging techniques, with both conventional and unconventional sources, and further improvements and automation of the analysis part will play an important role in achieving a better knowledge of the mechanisms related to soil microaggregates, especially when coupled with techniques aimed at describing the distribution of the different microbial communities.

***Acknowledgement***

The authors acknowledge the Advanced Light Source staff at BL 8.3.2. Dula Parkinson and Alastair MacDowell for the help with the beamline setup. The Advanced Light Source is supported by the Director, Office of Science, Office of Basic Energy Sciences, of the U.S. Department of Energy under Contract No. DE-AC02-05CH11231. This work has been founded through the Lawrence Berkeley National Laboratory Directed Research and Development (LDRD) "Integrative mapping of soil heterogeneity at the microbial scale" #366197. We thank an anonymous reviewer whose comments helped to improve and clarify this manuscript.

***References***

Accardo, A.P., Strolka, I., Toffanin, R., Vittur, F., 2005. Medical imaging analysis of the three dimensional (3D) architecture of trabecular bone: techniques and their applications. Medical Imaging Systems Technology-Methods in General Anatomy. Singapura: World Scientific Publishing Co. Pte. Ltd, 1-41.

Anderson, S.H., Peyton, R.L., Gantzer, C. J., 1990. Evaluation of constructed and natural soil macropores using X-ray computed tomography. Geoderma, 46(1), 13-29.

Anderson, A.N., Mcbratney, A.B., 1995. Soil aggregates as mass fractals. Aus. J. Soil Res. 33(5), 757-772.

Arzilli, F., Mancini, L., Voltolini, M., Cicconi, M.R., Mohammadi, S., Giuli, G., Mainprice, D., Paris, E., Barou, F. and Carroll, M.R., 2015. Near-liquidus growth of feldspar spherulites in trachytic melts: 3D morphologies and implications in crystallization mechanisms. Lithos, 216, 93-105.

Bachmann, F., Hielscher, R., Schaeben, H., 2010. Texture analysis with MTEX–free and open source software toolbox. Sol. St. Phen., 160, 63-68.

Bailey, V.L., McCue, L.A., Fansler, S.J., Boyanov, M.I., DeCarlo, F., Kemner, K.M. Konopka, A., 2013. Micrometer-scale physical structure and microbial composition of soil macroaggregates. Soil Biol. Biochem., 65, pp.60-68.

Bronnikov, A.V., 2002. Theory of quantitative phase-contrast computed tomography. JOSA A, 19(3), 472-480.

Bundt, M., Widmer, F., Pesaro, M., Zeyer, J., Blaser, P., 2001. Preferential flow paths: biological 'hot spots' in soils. Soil Biol. Biochem., 33(6), 729-738.

Chenu, C., Hassink, J., Bloem, J., 2001. Short-term changes in the spatial distribution of microorganisms in soil aggregates as affected by glucose addition. Biol. Fert. Soils, 34(5), 349-356.

Chenu, C., Stotzky, G., 2002. Interactions between microorganisms and soil particles: an overview. Interactions between soil particles and microorganisms: Impact on the terrestrial ecosystem. IUPAC. John Wiley and Sons, Ltd., Manchester, UK, pp.1-40.

Clausnitzer, V., Hopmans, J.W., 1999. Determination of phase-volume fractions from tomographic measurements in two-phase systems. Adv. Water Resour., 22(6), 577-584.

Currie, J.A., 1962. The importance of aeration in providing the right conditions for plant growth. J. Sci. Food. Agric., 13, pp. 380-385.

De Gryze, S., Jassogne, L., Six, J., Bossuyt, H., Wevers, M., Merckx, R., 2006. Pore structure changes during decomposition of fresh residue: X-ray tomography analyses. Geoderma, 134(1), 82-96.

Dougherty, R., Kunzelmann, K. H., 2007. Computing local thickness of 3D structures with ImageJ. Microsc. Microanal., 13(S02), 1678-1679.

Ebrahimi, A., Or, D., 2015. Hydration and diffusion processes shape microbial community organization and function in model soil aggregates. Water Resour. Res., 51, pp. 9804-9827.

Edwards, A. P., Bremner, J. M., 1967. Microaggragates in soils. J. Soil Sc., 18(1), 64-73.

Emerson, W.W., 1959. Stability of soil crumbs. Nature, 138, 538-538.

Foster, R.C., 1988. Microenvironments of soil microorganisms. Biol. Fert. Soils, 6(3), pp.189-203.

Gibson, J. R., Lin, H., Bruns, M. A., 2006. A comparison of fractal analytical methods on 2-and 3-dimensional computed tomographic scans of soil aggregates. Geoderma, 134(3), 335-348.

Gimenez, D., Perfect, E., Rawls, W. J., Pachepsky, Y., 1997. Fractal models for predicting soil hydraulic properties: a review. Eng. Geol., 48(3), 161-183.

Griffiths, R. S., and Young, I. M. 1994. The effects of soil structure on protozoa in a clay -loam soil. Eur. J. Soil Sc., 45(3), 285-292.

Heeraman, D. A., Hopmans, J. W., Clausnitzer, V., 1997. Three dimensional imaging of plant roots in situ with X-ray computed tomography. Plant Soil, 189(2), 167-179.

Heijs, A. W., De Lange, J., Schoute, J. F., Bouma, J., 1995. Computed tomography as a tool for non-destructive analysis of flow patterns in macroporous clay soils. Geoderma, 64(3), 183-196.

Hu, Q., Qian, G., Nowinski, W. L., 2005. Fast connected-component labelling in three-dimensional binary images based on iterative recursion. Comput. Vis. Image Und., 99(3), 414-434.

Kak, A.C., Slaney, M., 1987. Principles of Computerized Tomography, New York, IEEE Press.

Ketcham, R.A., Ryan, T.M., 2004. Quantification and visualization of anisotropy in trabecular bone. J. Microsc., 213(2), 158-171.

Khan, F., Enzmann, F., Kersten, M., Wiegmann, A., Steiner, K., 2012. 3D simulation of the permeability tensor in a soil aggregate on basis of nanotomographic imaging and LBE solver. J. Soils Sedim., 12(1), 86-96.

Lee, T.C., Kashyap, R.L., Chu, C.N., 1994. Building skeleton models via 3-D medial surface axis thinning algorithms. CVGIP: Graph. Model. Im. Proc., 56(6), 462-478.

Liebovitch, L.S., Toth, T., 1989. A fast algorithm to determine fractal dimensions by box counting. Phys. Lett. A, 141(8), 386-390.

Lindquist, W.B., Lee, S.M., Coker, D.A., Jones, K.W., Spanne, P., 1996. Medial axis analysis of void structure in three-dimensional tomographic images of porous media. J. Geophy. Res.-Sol. Ea. (1978–2012), 101(B4), 8297-8310.

Ma, R., Cai, C., Li, Z., Wang, J., Xiao, T., Peng, G., Yang, W., 2015. Evaluation of soil aggregate microstructure and stability under wetting and drying cycles in two Ultisols using synchrotron-based X-ray micro-computed tomography. Soil Till. Res., 149, 1-11.

Macedo, A., Crestana, S., Vaz, C.M.P., 1998. X-ray microtomography to investigate thin layers of soil clod. Soil Till. Res., 49(3), 249-253.

Menon, M., Yuan, Q., Jia, X., Dougill, A.J., Hoon, S.R., Thomas, A.D., Williams, R.A., 2011. Assessment of physical and hydrological properties of biological soil crusts using X-ray microtomography and modeling. J. Hydrol., 397(1), 47-54.

McBratney, A.B., 1993. Comments on "Fractal Dimensions of Soil Aggregate-Size Distributions Calculated by Number and Mass". Soil Sci. Soc. Am. J., 57(5), 1393-1393.

McCarthy, J.F., Ilavsky, J., Jastrow, J.D., Mayer, L.M., Perfect, E. Zhuang, J., 2008. Protection of organic carbon in soil microaggregates via restructuring of aggregate porosity and filling of pores with accumulating organic matter. Geochim. Cosmochim. Ac., 72(19), pp.4725-4744.

Molins, S., Trebotich, D., Steefel, C.I., Shen, C., 2012. An investigation of the effect of pore scale flow on average geochemical reaction rates using direct numerical simulation. Water Resour. Res. 48(W03527).

Mooney, S.J., Pridmore, T.P., Helliwell, J., Bennett, M.J., 2012. Developing X-ray Computed Tomography to non-invasively image 3-D root systems architecture in soil. Plant Soil, 352(1-2), 1-22.

Nunan, N., Ritz, K., Rivers, M., Feeney, D.S., Young, I.M., 2006. Investigating microbial micro-habitat structure using X-ray computed tomography. Geoderma, 133(3), 398-407.

Oades, J.M., 1984. Soil organic matter and structural stability: mechanisms and implications for management. Plant Soil, 76(1-3), 319-337.

Odgaard, A., 1997. Three-dimensional methods for quantification of cancellous bone architecture. Bone, 20(4), 315-328.

Odgaard, A., Kabel, J., van Rietbergen, B., Dalstra, M., Huiskes, R., 1997. Fabric and elastic principal directions of cancellous bone are closely related. J. Biomech., 30(5), 487-495.

Ohser, J., Mücklich, F., 2000. Statistical analysis of microstructures in materials science. Chichester: Wiley.

Or, D., Smets, B.F., Wraith, J.M., Dechesne, A., Friedman, S.P., 2007. Physical constraints affecting bacterial habitats and activity in unsaturated porous media–a review. Adv. Water Resour., 30(6), pp.1505-1527.

Paganin, D., Mayo, S.C., Gureyev, T.E., Miller, P.R., Wilkins, S.W., 2002. Simultaneous phase and amplitude extraction from a single defocused image of a homogeneous object. J. Microsc., 206(1), 33-40.

Palágyi, K., Kuba, A., 1999. A parallel 3D 12-subiteration thinning algorithm. Graph. Model Im. Proc., 61(4), 199-221.

Parfitt, A.M., Drezner, M.K., Glorieux, F.H., Kanis, J.A., Malluche, H., Meunier, P.J., Ott, S.M., Recker, R.R., 1987. Bone histomorphometry: standardization of nomenclature, symbols, and units: report of the ASBMR Histomorphometry Nomenclature Committee. J. Bone Miner. Res., 2(6), 595-610.

Perfect, E., Rasiah, V., Kay, B.D., 1992. Fractal dimensions of soil aggregate-size distributions calculated by number and mass. Soil Sc. Soc. Am. J., 56(5), 1407-1409.

Peth, S., Horn, R., Beckmann, F., Donath, T., Smucker, A.J., 2008, August. The interior of soil aggregates investigated by synchrotron-radiation-based microtomography. In Optical Engineering+ Applications (pp. 70781H-70781H). International Society for Optics and Photonics.

Peth, S., Horn, R., Beckmann, F., Donath, T., Fischer, J., Smucker, A.J. M., 2008. Three-dimensional quantification of intra-aggregate pore-space features using synchrotron-radiation-based microtomography. Soil Sc. Soc. Am. J., 72(4), 897-907.

Peth, S., Chenu, C., Leblond, N., Mordhorst, A., Garnier, P., Nunan, N., Pot, V., Ogurreck, M., Beckmann, F., 2014. Localization of soil organic matter in soil aggregates using synchrotron-based X-ray microtomography. Soil Biol. and Biochem., 78, pp.189-194.

Petrovic, A.M., Siebert, J.E., Rieke, P.E., 1982. Soil bulk density analysis in three dimensions by computed tomographic scanning. Soil Sci. Soc. Am. J., 46(3), 445-450.

Peyton, R.L., Haeffner, B.A., Anderson, S.H., Gantzer, C.J., 1992. Applying X-ray CT to measure macropore diameters in undisturbed soil cores. Geoderma, 53(3), 329-340.

Peyton, R.L., Gantzer, C.J., Anderson, S.H., Haeffner, B.A., Pfeifer, P., 1994. Fractal dimension to describe soil macropore structure using X ray computed tomography. Water Resour. Res., 30(3), 691-700.

Phillips, J.D., 2009. Soils as extended composite phenotypes. Geoderma, 149(1), pp.143-151.

Pierret, A., Capowiez, Y., Belzunces, L., Moran, C. J., 2002. 3D reconstruction and quantification of macropores using X-ray computed tomography and image analysis. Geoderma, 106(3), 247-271.

Ranjard, L., Nazaret, S., Gourbière, F., Thioulouse, J., Linet, P., Richaume, A., 2000. A soil microscale study to reveal the heterogeneity of Hg (II) impact on indigenous bacteria by quantification of adapted phenotypes and analysis of community DNA fingerprints. FEMS Microbiol. Ecol., 31(2), 107-115.

Remenant, B., Grundmann, G.L., L. Jocteur-Monrozier., 2009. From the micro-scale to the habitat: Assessment of soil bacterial community structure as shown by soil structure directed sampling, Soil Biol. Biochem., 41, pp. 29-36.

Renault, P., Stengel, P., 1994. Modeling Oxygen Diffusion in Aggregated Soils: I. Anaerobiosis inside the Aggregates, Soil Sci. Soc. Am. J., 58, pp. 1017-1023.

Russ, J. C., DeHoff, R. T. 2012 Practical stereology. Springer Science & Business Media.

Schindelin, J., Arganda-Carreras, I., Frise, E., Kaynig, V., Longair, M., Pietzsch, T., Cardona, A. 2012. Fiji: an open-source platform for biological-image analysis. Nature Methods, 9(7), 676-682.

Silin, D., Tomutsa, L., Benson, S.M., Patzek, T.W. 2010 Microtomography and pore-scale modeling of two-phase fluid distribution. Transport Porous Med., 86(2), 495-515.

Simmons, C.A., Hipp, J.A., 1997. Method-based differences in the automated analysis of the three-dimensional morphology of trabecular bone. J. Bone Miner. Res., 12(6), 942-947.

Six, J., Paustian, K., Elliott, E.T., Combrink, C., 2000. Soil structure and organic matter I. Distribution of aggregate-size classes and aggregate-associated carbon. Soil Sci. Soc. Am. J., 64(2), 681-689.

Six, J.A.E.T., Elliott, E.T., Paustian, K., 2000. Soil macroaggregate turnover and microaggregate formation: a mechanism for C sequestration under no-tillage agriculture. Soil Biol. Biochem., 32(14), pp.2099-2103.

Six, J., Bossuyt, H., Degryze, S., Denef, K., 2004. A history of research on the link between (micro) aggregates, soil biota, and soil organic matter dynamics. Soil Till. Res., 79(1), 7-31.

Sleutel, S., Cnudde, V., Masschaele, B., Vlassenbroek, J., Dierick, M., Van Hoorebeke, L., De Neve, S., 2008. Comparison of different nano-and micro-focus X-ray computed tomography set-ups for the visualization of the soil microstructure and soil organic matter. Comput. Geosci., 34(8), 931-938.

Smith, K.A., 1980. A model of the extent of anaerobic zones in aggregates soils, and its potential application to estimates of denitrification. J. Soil Sci., 31, pp. 263-277.

Spanne, P., Jones, K.W., Prunty, L., Anderson, S.H., 1994. Potential applications of synchrotron computed microtomography to soil science. Tomography of Soil-Water-Root Processes (Conference Proceedings), 43-57.

Tisdall, J.M., Oades, J., 1982. Organic matter and water-stable aggregates in soils. J. Soil Sci., 33(2), 141-163.

Vargas, R., Hattori, T., 1986. Protozoan predation of bacterial cells in soil aggregates. FEMS Microbiol. Ecol., 38, pp. 233-242.

Vogel, C., Mueller, C.W., Höschen, C., Buegger, F., Heister, K., Schulz, S., Schloter, M., Kögel-Knabner, I., 2014. Submicron structures provide preferential spots for carbon and nitrogen sequestration in soils. Nature Comm., 5.

Voltolini, M., Zandomeneghi, D., Mancini, L., Polacci, M., 2011. Texture analysis of volcanic rock samples: Quantitative study of crystals and vesicles shape preferred orientation from X-ray microtomography data. J. Volcanol. Geoth. Res., 202(1), 83-95.

~~Voltolini, M., Kwon T.-H., Ajo-Franklin J., 2017. Visualization and Prediction of Supercritical $CO_2$ Distribution in Sandstones during the Invasion: Contributions to Geological Carbon Sequestration from an in situ Synchrotron X-Ray micro-Computed Tomography. Submitted to the International Journal of Greenhouse Gas Control.~~

Weitkamp, T., Haas, D., Wegrzynek, D., Rack, A., 2011. ANKAphase: software for single-distance phase retrieval from inline X-ray phase-contrast radiographs. J. Synchrotron Radiat., 18(4), 617-629.

Whitehouse, W.J., 1974. The quantitative morphology of anisotropic trabecular bone. J. Microsc., 101(2), 153-168.

Wright, D.A., Killham, K., Glover, L.A., Prosser, J.I., 1995. Role of Pore Size Location in Determining Bacterial Activity during Predation by Protozoa in Soil. Appl. Environ. Microbiol., 61(10), 3537-3543.

Young, I. M., Ritz, K., 1998. Can there be a contemporary ecological dimension to soil biology without a habitat? Soil Biol. Biochem., 30(10-11), 1229-1232.

Young, I.M., Crawford, J.W., 1991. The fractal structure of soil aggregates: its measurement and interpretation, J. Soil Sci., 42, 187-192.

Young, I.M., Crawford, J.W., 2004. Interactions and self-organization in the soil-microbe complex. Science, 304(5677), 1634-1637.

Yushkevich, P.A., Piven, J., Hazlett, H.C., Smith, R.G., Ho, S., Gee, J.C., Gerig, G., 2006. User-guided 3D active contour segmentation of anatomical structures: significantly improved efficiency and reliability. Neuroimage, 31(3), 1116-1128.

Zhou, H., Peng, X., Perfect, E., Xiao, T., Peng, G., 2013. Effects of organic and inorganic fertilization on soil aggregation in an Ultisol as characterized by synchrotron based X-ray micro-computed tomography. Geoderma, 195, 23-30.

***Figure Captions***

Figure 1.

Whole and vertically cut volume renderings of the Kansas and Barrow soil microaggregates.

Figure 2.

Barrow microaggregate showing the calculated "outer surface" (displayed in red), in a vertically cut sample with a partial covering of the surface (a), and a thin slice with the surface following the outer border (b).

Figure 3.

The two microaggregates showing the local thickness volume superimposed to the 8bit volume rendering and alone. Volumes are cut to better show the internal features.

Figure 4.

Frequency plots showing the distribution of (from top to bottom): local thickness voxels, skeleton branch lengths, surface openings.

Figure 5.

Pore space accessibility from the outside for spherical structuring elements of different sizes: .65 μm (yellow), 2 μm (green), 10 μm (red).

Figure 6.

Renderings of the skeletons, displayed superimposed both with a cut 8bit volume and alone. The skeleton is labeled with the local thickness values for each voxel.

Figure 7.

Analysis of openings: the rendering on the left for the two microaggregates shows the 8bit rendering with the openings marked bi cubes labeled with respect their size. On the right the skeleton and the openings alone are plotted.

Figure 8.

Star Length Distribution analysis for anisotropy characterization. The SLD analysis has been carried out on both the solids of the microaggregates (PF's on the left) and the whole completely filled aggregate (PF's on the right). Values are in multiples of random distribution, PF's are in equal area projection, upper hemisphere. The bottom of the figure shows the whole and horizontally sectioned microaggregates oriented as the PF's.

Figure 9.

Thin horizontal slice of the two samples showing in more details and summarizing the main analyses carried out on the microaggregates.

Table 1. Morphometric analysis.

| | ***Kansas*** | ***Barrow*** |
|---|---|---|
| *Volumetric Analysis* | | |
| Total Aggregate Volume [$\mu m^3$] | 2.819E+06 | 3.619E+06 |
| Total Volume of solids [$\mu m^3$] | 1.970E+06 | 1.998E+06 |
| Total Volume of voids [$\mu m^3$] | 8.486E+05 | 1.621E+06 |
| Porosity [%] | 43.1 | 81.1 |
| *Surface Area Analysis* | | |
| Surface Area [$\mu m^2$] | 3.505E+06 | 4.850E+06 |
| SNSVR | 11.8 | 13.8 |
| *Minkowski Functionals and Fractal Analysis* | | |
| Integral of mean curvature (solids) [$\mu m^{-2}$] | -45197.6 | -21798.8 |
| Euler Characteristic (voids) [$\mu m^{-3}$] | -312.6 | -410.6 |
| Fractal dimension 3D (voids) | 2.353 | 2.401 |
| *Local Thickness Analysis* | | |
| Structure Separation Mean [μm] | 3.13 | 5.32 |
| Structure Separation σ [μm] | 1.89 | 4.13 |
| Structure Separation Max [μm] | 12.77 | 24.74 |
| Structure Thickness Mean [μm] | 6.46 | 7.45 |
| Structure Thickness σ [μm] | 5.44 | 11.44 |
| Structure Thickness Max [μm] | 28.66 | 47.07 |
| *Geometrical Accessibility Analysis* | | |
| 0.65 μm elements accessibility [% of voids] | 95.5 | 98.0 |
| 2 μm elements accessibility [% of voids] | 76.0 | 86.2 |
| 10 μm elements accessibility [% of voids] | 0 | 3.2 |
| *Anisotropy analysis SLD -solids-* | | |
| Isotropy index (I) | 0.937 | 0.763 |
| Elongation index (E) | 0.019 | 0.153 |

Table 2. Skeleton analysis

| | ***Kansas*** | ***Barrow*** |
|---|---|---|
| Number of branches | 54550 | 81012 |
| Number of true junctions | 29752 | 44202 |
| Number of end points | 11143 | 13552 |
| Number of triple points | 23113 | 33105 |
| Number of quadruple points | 4953 | 7713 |
| Average branch length [μm] | 3.41 | 3.40 |

| | | |
|---|---|---|
| Max branch length [μm] | 24.54 | 46.07 |

## Highlights

- Synchrotron X-ray tomography of whole soil aggregates at unprecedented resolution.
- Advanced image processing for quantitative soil microaggregates characterization.
- Modeling of the morphological accessibility for ideal microorganisms.

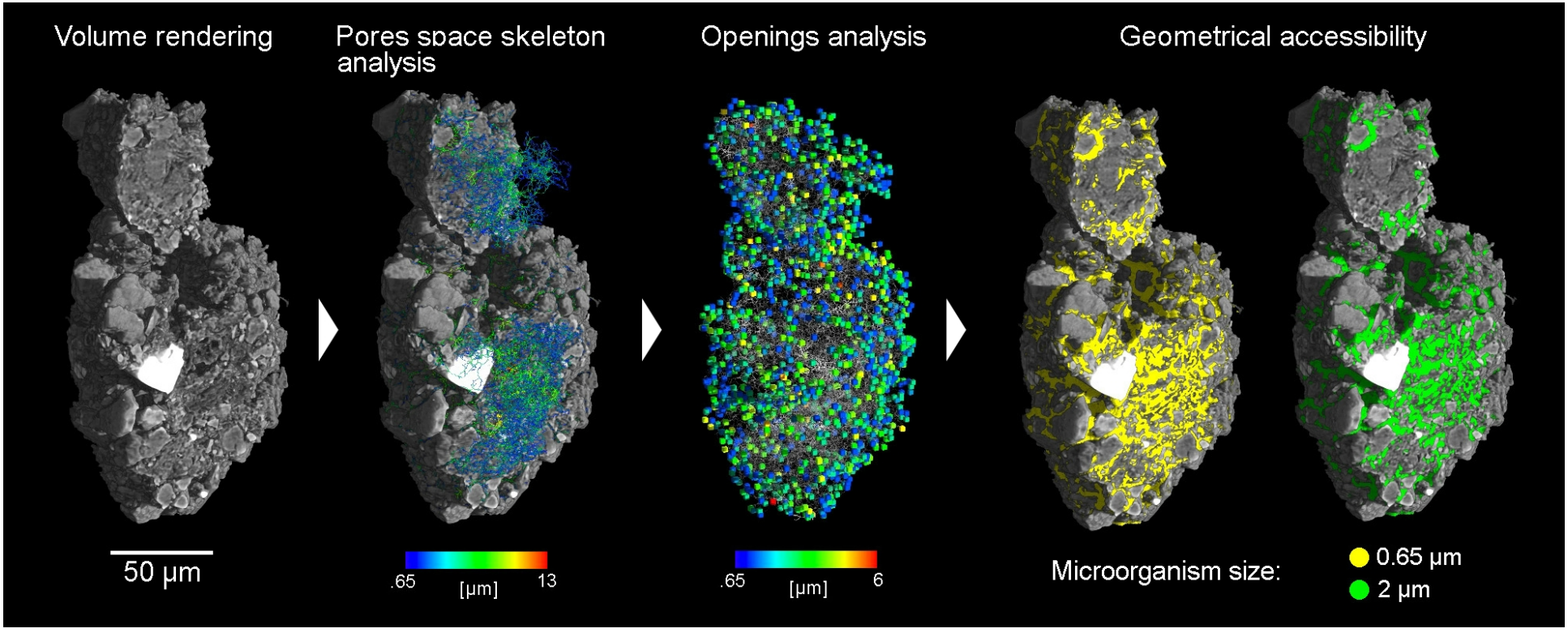
Volume rendering
Pores space skeleton analysis
Openings analysis
Geometrical accessibility
50 µm
.65
[µm]
13
.65
[µm]
6
Microorganism size:
0.65 µm
2 µm

# *Quantitative characterization of soil micro-aggregates: new opportunities from sub-micron resolution synchrotron X-ray microtomography*

Marco Voltolini[1], Neslihan Taş[1], Shi Wang[1], Eoin L. Brodie[1,2], Jonathan B. Ajo-Franklin[1]

[1] Earth and Environmental Sciences, Lawrence Berkeley National Laboratory, Berkeley, CA 94720.

[2] Department of Environmental Science Policy and Management, University of California, Berkeley, CA 94720.

***Abstract***

Soil microaggragates are the fundamental building block, at the micron scale, of the highly hierarchical structure of soils, and can exert a significant control on the local biological metabolism and microbial community partitioning. In this study we propose an analysis protocol for the morphometric characterization of complete soil microaggregates based on sub-micron resolution synchrotron X-ray microtomography. A comprehensive characterization of the aggregate morphology is the first step towards a complete characterization of the soil microaggregates, when trying to correlate morphometric parameters with physical and/or biological properties, or when building models (e.g.,

effective diffusivity, microbial distribution, etc.). We demonstrate our characterization approach on two single microaggregate samples from dramatically different soil environments: one from Kansas, primarily composed by inorganic particles, and one from Barrow (Alaska) dominated by plant fragments. A series of state-of-the-art morphometric analysis techniques have been employed providing quantitative results highlighting specific differences of the two samples. The role of the microstructure in a scenario microbial population development has been discussed and it has been found that the Barrow microaggregate seems to be more favorable, from a purely geometrical point of view, as also confirmed by a simple model presented in this work. The potential of this approach, when coupled with chemical and biological analysis for a fully comprehensive characterization of soil aggregates in the larger picture of enhanced biological activity, is evident.

*Keywords: Synchrotron X-Ray microCT; Soil microaggregate; Quantitative image analysis; Modeling.*

## *1. Introduction*

Soil is perhaps the ultimate "complex system", with physical, chemical and biological components interacting in a non-linear manner yet displaying clear properties of co-evolution and self-organization (Young and Crawford, 2004). The physical structure of soil acts in a deterministic manner to regulate the assembly and activity of soil biota, including microorganisms, and through their activity, soil biota continuously shape and

re-form both the macroscale and microscale structure of soil that in turn poses new constraints on biological activity. This pattern of co-evolution has led to the concept of soils being considered as 'extended composite phenotypes', (Phillips, 2009) where soils themselves "*are an expression of the cumulative impacts of the biosphere on surface processes*". As the fundamental units of soil, aggregates and their physical, chemical, and biological properties could be considered an extended soil phenotype.

The aggregation properties of soil constituents lead to a classification of aggregate forms, primarily based on size and basic physical properties (e.g., stability in water, Six et al., 2000). Microaggregates, those less than 250 μm in diameter (Edwards and Bremner, 1967) are critical for the sequestration of carbon in soil (e.g., Six et al., 2000, 2004, Vogel et al., 2014). Within microaggregates, pore structural properties that evolve during aggregate formation and stabilization result in organic matter being encapsulated within submicron pores (McCarthy et al., 2008) and, thus, protected from microbial decomposition due to kinetic and spatial constraints. Given its importance, the relationship between pore space geometry on the diversity and activity of soil microorganisms has been a topic of notable interest (reviewed in Or et al., 2007). Significant fractions of soil pore space can be inaccessible to soil bacteria (Chenu and Stotzky, 2002), and observations of bacteria confined within pore spaces are common (Foster et al., 1988), while predators such as protozoa can be isolated from their bacterial prey due to the interaction between pore geometry and the larger cell dimensions of protozoa (Vargas & Hattori, 1986, Wright et al., 1995).

Perhaps the strongest constraints on microbial metabolism within microaggregates are those of gas, moisture, and solute transport. Diffusive gas transport in particular is

limited by the aperture and connectivity of exterior pores to deeper environments as well as pore hydration state. In the near-surface, anoxic microenvironments can develop in the interior of microaggregates due to $O_2$ diffusion limitations as well as aerobic communities on aggregate surfaces. Due to the difficulties in measuring spatial concentrations gradients within microaggregates, many studies exploring these constraints focus on modeling approaches (Currie, 1962; Smith, 1980; Renault & Stengel. 1994; Ebrahimi & Or, 2015). Currie (1962) and Smith (1980) provide 1D continuum analytical models for such processes which are strongly dependent on an averaged $D_{eff}$, the effective gas diffusivity of the aggregate. Aggregate-specific $D_{eff}$ values are difficult to estimate, particularly for partial saturation states where capillary-bound water impacts gas transport. Ebrahimi and Or (2015) present a pore-resolved numerical model of gas and nutrient diffusion in microbially active aggregates and demonstrate that aerobic and anaerobic microenvironments quickly develop; such spatial gradients in turn drive community partitioning, particularly in wetter environments. A common limitation of all such studies is the absence of realistically parameterized pore geometries, particularly for microbially "remodeled" aggregates which are unlikely to have homogeneous network structures as shown in prior imaging studies (e.g., Peth et al. 2008, Alba-Tercedor et al. 2015).

Given the importance of soil pore geometry and pore network connectivity for biodiversity and biogeochemical cycling, it is critical to develop quantitative measurement approaches to obtain soil aggregate microstructure at the relevant length scales (i.e. sub-micron). The microstructure of these fundamental soil building blocks will likely have a significant impact on the ability to host specific microorganisms; for

example large pores with many small apertures can provide a safe environment for specific microorganism colonies to thrive. The direct correlation of microstructure and microorganism distribution is beyond the scope of this work, which focuses in on development of morphometric parameters and analysis strategies to obtain a comprehensive description of the microstructure of soil microaggregates. Our results do, however, provide insight into prior experimental studies examining the role of microaggregates in disrupting predation (Wright et al. 1995, Vargas and Hattori, 1986).

A first attempt at correlating Synchrotron X-Ray micro-Computed Tomography (SXR-μCT) data with microbial populations obtained via 16S rRNA pyrosequencing has been attempted in Bailey et al. (2013), where no clear correlation of microbial populations with microstructure has been found. While that work is valid, the lack of an advanced analysis of the SXR-μCT data (only proxies of pore size distributions and surface areas have been considered as descriptors for the microstructure) might have neglected important hints that could have been successful in finding an eventual correlation. In this context, we are offering an example of a state-of-the-art measurement and data analysis that can be used for a complete characterization of *whole* (in contrast with cropped subvolumes, as usually found in literature) soil microaggregates at the nanoscale, providing the soil scientist community a series of tools that can be used in future works where a comprehensive *quantitative* characterization of soil microaggregates is needed.

XR-CT (both using conventional and unconventional radiation sources, at different scales) has been successfully used for soil characterization in the past, given its ability to provide 3D volumes describing the structure soil samples. One of the main

advantages of this technique is its non-destructive nature, which allows the observation of undisturbed samples, such as roots in soils (Heerman et al., 1997; Mooney et al., 2013), macropores in large (~20 cm) soil cores (Pierret et al., 2002), and characterization of pore space in ~3 mm aggregates (Nunan et al., 2006; Peth et al., 2008). More specific works, focusing on the characterization of the pore networks in soils, at different scales, can be found in Petrovic et al. (1982), and Anderson et al. (1990) where the main focus was the estimate of the density of the soil samples. At the mm scale, XR-CT has also been used to locate layering in soil samples as presented by Macedo et al. (1998). Other studies included porosity and flow properties in measured soils, as presented in Peyton et al. (1992), Heijs et al. (1995), Clausnitzer and Hopmans (2000). Fractal properties in soils have been studied although their calculation and practical implications have been somewhat controversial. Examples can be found in: Perfect et al., (1992), McBratney (1993), Peyton et al., (1994), Anderson and McBratney (2005), Gimenez et al., (1997), Gibson et al. (2006).

In this work we present state-of-the-art data processing and morphometric analysis of two different soil microaggregates (slightly smaller than 250 μm) to quantify microstructural attributes. The purpose is to show an analytical protocol that can be used to describe the microstructure of the soil microaggregates in a quantitative fashion, and to provide the scientific community (e.g., modelers) with datasets of *complete* microaggregate particles with sub-micron resolution to be used as a realistic starting point and/or validating dataset for synthetic soil models. To validate this approach, we have chosen two markedly different soil microaggregates, both in composition and texture, the first rich in inorganic material and the second rich in organic material (plant fragments) to better monitor which

parameters can describe those differences. This quantitative description of the soil microaggregates is fundamental for a complete study complementing the role of the soil microaggregates microstructure, chemical heterogeneities, and microorganism distributions in the research about the origin and development of "hot spots" in soils, and to contribute to our understanding of the functional stability and spatial variability within soils in general.

## *2. Materials and Methods*

### *2.1 Sample choice and preparation*

Two distinct soils were selected for our study: one from the Konza Prairie Biological Station, Kansas, and a second from Barrow Experimental Observatory (BEO), Alaska. The two samples selected for this evaluation varied in bulk density, organic matter content, and mineralogy, among other parameters. Microaggregates were obtained via manual dissection under a microscope, where the sorting was based on size (200 to 250 μm diameter), and on the ability to remain coherent under mechanical stimulation. Preparation of the aggregates for analysis involved inserting the microaggregates into a thin walled 300 μm borosilicate glass capillary (Charles Supper); the capillary tubes were immediately sealed using hard wax to maintain the original humidity as much as possible. The capillary tube was used to assist sample mounting and to maintain sample integrity at proper moisture conditions. Sealing and acclimation (~1 hour) at the synchrotron

beamline experimental hutch prior to the experiment is fundamental to keep the soil aggregate at proper conditions and avoid motion artifacts due to variations in humidity during the scan. The very high resolution of the measurement makes the dataset prone to motion artifacts, so a nearly perfectly stable sample was a necessity.

*2.2 SXR-μCT measurement and data reconstruction*

The SXR-μCT experiments were carried out at X-ray Imaging Beamline 8.3.2 (BL 8.3.2) at the Advanced Light Source (ALS) at the Lawrence Berkeley National Laboratory (LBNL). For the tomographic measurement, a 11 keV monochromatic beam was selected via a multilayer monochromator. The glass capillary containing the individual aggregates was mounted on a rotating stage, ~8 mm from the scintillator of the detector system; a short distance was selected to avoid strong phase-contrast effects due to free space propagation of the highly coherent XR beam. The detector system consisted of a LuAG 20 μm thick scintillator mounted in front of a 20× objective lens; the visible light signal obtained from the scintillator was recorded on a CCD camera (Optique Peter, Lentilly, France) obtaining a dataset with a resulting voxel size of 325 nm. 1800 projections were recorded for each sample over a 180° rotation, and the exposure time was 1 second per projection.

Before reconstruction of tomographic 2D slices, a single-distance phase retrieval algorithm was applied to the projection datasets. Phase-retrieval is beneficial in this kind of datasets since it improves the contrast between the different phases and makes the phase-contrast artifacts less pronounced, both these characteristics are of great help with

the segmentation via thresholding process. After a conventional flat-field correction of the single projection, we applied the Paganin single-distance phase retrieval algorithm (Paganin et al, 2002) as implemented in the ImageJ plugin ANKAPhase (Weitkamp et al., 2011), which proved to be effective (e.g., Arzilli et al., 2015) with datasets collected in the near-field Fresnel diffraction region (Bronnkov, 2002). After phase-retrieval the slices were reconstructed with a conventional filtered back-projection algorithm (Kak and Slaney, 1987).

Once the stacks of slices were reconstructed, the datasets were manually cropped to isolate the soil microaggregate, separating it from the glass capillary, to obtain an 8 bit grayscale volume used as a starting point for subsequent analysis. The volume rendering of the two particles, whole and with a virtual vertical cut to show the internal structure, are shown in Figure 1. It is immediately possible to qualitatively appreciate the microstructural differences and identify in the "Barrow" microaggregate a large amount of material originating from plant debris, visible as a cellular texture with large interior pores (right panel). In contrast, the microaggregate obtained from the Kansas prairie site (left panel) appears to be an aggregate of mineral particles with smaller interior pore spaces, displaying a more interstitial type of pore space.

*2.3 Data treatment and separation*

To allow analysis of pore-space morphologies, the first step in our analytical approach is segmentation, aimed at separating the phases of interest into binary volumes. A simple manual thresholding procedure was possible due to the strong contrast between the solid

and voids voxels in the samples obtained after the phase retrieval procedure. However, the analysis of microaggregates requires a deviation from classical approaches for segmentation commonly applied to XR-CT datasets. In most situations, the image volume is cropped and only a subsection of the system is segmented and analyzed. In our case we wanted to capture the entire particle and determine the properties of the aggregate exterior surface. This boundary forms the interface between the aggregate and the outside world and is key to imposing boundary conditions when looking for interactions of the outside with the microaggregate pore space, for example in gas transport modeling, predation, etc. This approach comes with a challenge, mainly the problem of separating the air outside the microaggregate from the air in the voids inside the sample despite the fact that the phases are continuous. This cannot be done via thresholding procedures, since the air inside and outside the sample has of course the same XR attenuation values (translated into the same grayscale value, in the tomographic dataset), thus the necessity of morphology-based methods.

We have developed an iterative procedure using the Fiji software framework (Schindelin et al., 2012) that allows the calculation of such an external surface and provides a separation of the pore space from the air outside the sample. This procedure can produce results similar in concept to the snake-based "active contour" segmentation algorithms used in the medical imaging field (e.g., Yushkevich et al., 2006). The procedure we applied works well in 3D and can be applied to systems where large objects need to be extracted and segmented. The procedure consists of a series of operations involving local thickness (LT) analysis of the voids using the plugin described in Dougherty and Kunzelmann (2007). LT analysis is used to obtain a first, rough, outer

surface and a closing procedure is used to close the smaller outer pores. 3D void filling is then used to fill the largest internal voids, and finally masking is utilized to preserve the small features that are commonly erased by the morphological operators such as eroding and dilating processes. The filled soil aggregate particle obtained is then used to obtain a "sample surface" again through morphological operators of the binary erosion/dilation class coupled with Boolean operations. This outer surface obtained with the procedure described above is shown in Figure 2 rendered in red and superimposed on a rendering of the Barrow sample. The virtual cuts reveal how the surface calculation effectively "wraps" the aggregate exterior without penetrating into the interior pore spaces, thus providing information on the interface between the aggregate and the surrounding environment. The procedure of calculating a surface separating the pore space from the outer air is the starting point for subsequent analyses on the two datasets.

## ***Results***

### *3.1 Morphometric analysis: Basic analysis*

The procedure described above generates two base binary volumes for the morphometric analysis: a volume for inner voids (the pore space) and a volume of the solid phase. This allows a variety of analytical techniques to be carried out in order to obtain quantitative information describing the two different phases. We stress that all the morphometric analysis needs to be considered with the actual resolution of the measurement in mind;

some values (such as surface area values) are very sensitive to image resolution and the value listed must be read with this intrinsic limitation in mind. For SXR-μCT anaylsis, a compromise between field of view and resolution needs to be made; we have chosen the setup with the ability to image the whole soil microaggregate with the highest resolution possible. With the chosen setup the resolution was very high, especially when compared to similar measurements presented in literature, but still without the ability to resolve the smallest features (e.g., single clay minerals platelets). We present a comparison of a range of classical morphometric metrics applied to our two samples, including porosity, surface area, sphere-normalized surface-area-to-volume-ratio, Minkowski functionals, and fractal dimension metrics; such metrics provide a first step in grouping aggregate properties.

The first analysis carried out was to calculate the basic properties of the aggregates, such as their volumes and porosities. In Table 1, a summary of the morphometric analyses carried out on the two samples is listed. From the volumetric analysis, we can see how the Barrow sample is ~22% larger in volume than the Kansas one. The cellular texture and interior pores seen in the Barrow sample results in a high porosity (81%) while the Kansas aggregate has a porosity more typical of granular composites (43%). The surface area (SA) calculation also shows a higher value for the Barrow sample but the impact of sample size makes such a non-normalized SA problematic to interpret. To overcome this problem a sphere-normalized surface-to-area volume ratio (SNSVR) was calculated with SNSVR defined as $SA_{obj}/SA_{sph}$. $SA_{obj}$ is the object surface area, and $SA_{sph}$ is the surface area of a sphere with the same volume of the object. The farther the object surface is from a spherical surface, the higher the SNSVR

value (1 being the value for a perfect sphere). After this correction, the Barrow sample still shows a larger area available per volume units, but both the microaggregate particles display values related to a markedly complex surface.

The Minkowski functionals (see e.g., Ohser and Muecklich, 2000) can be used as topological descriptors of a binarized volume. More specifically the integral mean curvature (IMC) (Russ and DeHoff, 2012) is a value related to the concavity/convexity (depending on the sign of the IMC) of the surfaces present in the sample. The Euler characteristic (EC) (Odgaard and Gundersen, 1996) is a value related to the connectivity of the objects in the volume: positive values mean isolated objects, while connected networks generally display negative values. The values measured for the IMC of the framework of solids and the EC of the pore space highlight a highly connected network dominated by concave shapes of the solid framework, with the Barrow sample being slightly more interconnected and with a slightly weaker dominance of convex surfaces.

Another frequently used parameter for texture analysis is the fractal dimension (FD), which has been applied to the solids in the aggregate, providing an index of self-similarity of the microstructural features at different scales. The FD has been calculated using the box-counting method (Liebovitch and Toth, 1989) and values obtained show that the Barrow aggregate (FD = 2.401) is slightly more self-similar than Kansas sample (FD = 2.353). Both values are relatively low (for volume data $2 \leq FD \leq 3$) highlighting moderate fractal properties, at the considered resolution and sample size. Prior studies examining the fractal dimension of micro-aggregates using destructive mass/radius analysis have yielded slightly higher values (FD = 2.75 to 2.93, Young & Crawford,

1991), the differences in sample origin and measurement approach make comparisons challenging.

*3.2 Local thickness (LT) analysis*

As discussed in section 2.3, LT analysis is an extremely useful approach for porous material characterization borrowed from the bone scientist community, where it is generally used for the analysis of cancellous bone, measuring parameters such as the "trabecular thickness" and "trabecular separation" (Parfitt et al., 1987; Simmons and Hipp, 1997; Accardo et al., 2005). The same algorithm has been later adopted in different contexts for example as part of multiphase flow modeling approaches by Silin et al. (2010) under the name "maximum inscribed spheres" and is finding increased use in modeling of geologic samples. The term "local thickness" for a voxel is used to mean the diameter of the maximum inscribed sphere in the structure that contains the voxel. In Table 1., where the LT results are summarized, we use more generic terms, where "structure separation" is the LT analysis calculated on the pore space volume, while with "structure thickness" we mean the LT analysis carried out on the solid framework. The analysis has been performed using the Fiji plugin from Dougherty and Kunzelmann (2007), and graphical results are shown in Figure 3 for both the migroaggregates.

In Figure 3 a vertically cut rendering is superimposed with the LT-labeled volume of the pore space, and a volume rendering of the cut LT volume itself. The image clearly displays the thickness variations of the pore space within the volume, with the Kansas sample showing interstitial voids created by the aggregation of the silt particles, while in

Barrow the larger, smoother, voids due to the presence the plant fragments and their cellular structures are evident. A larger variation of LT values is also immediately observable from the renderings in figure. A quantification of the LT analysis was performed and the results are presented again in Table 1. The mean of the structure separation (mean LT of the pore space) is larger in the Barrow sample, but also the standard deviation is significantly larger and the maximum LT value of voids is present in the Barrow sample as well, this again because of the presence of the plant fragments with large voids surrounded by small ones. This variability is recognizable when looking at more detailed data than the one summarized in the Table 1. In Figure 4 we show a plot of the LT values distribution in the pore space for both Kansas and barrow. The higher variability suggested by the summarizing values here becomes even more evident with the two distributions being markedly different, with values of higher LT values being more frequent in the Barrow sample. The smallest LT values are also more frequent in the Barrow sample, while the small LT values are generally more frequent in the Kansas microaggregate, showing a sharper LT distribution curve. This feature and its implications are discussed in section 4.

Concerning the structure LT analysis ("structure thickness") values for Barrow are generally slightly larger, with a much larger standard deviation value and especially a larger maximum. This because in the Barrow sample a ~50 μm large single mineral particle is present (top of the sample).

*3.3 Geometrical accessibility analysis*

The concept of LT, combined with the outer surface calculated via the procedure described above, and the connected component labeling (CCL, see e.g., Hu et al. 2005) can be used to calculate the parts of the sample accessible from the outside by objects with different sizes. This class of analysis has obvious applications as a simple model able to provide insights about pore-size constrained microbial colonization of aggregates, as well as the spatial limits of predation by larger organisms. The procedure is straightforward: a threshold value (corresponding to the size of the structuring element - spherical- considered for accessibility) is applied to the LT volume. A 5 voxel thick outer surface is added to the volume and a CCL procedure is initiated starting from the outer surface; this will find all the parts of the sample accessible from the outside. The outer surface is then removed using a masking procedure with the pore space binary volume. The volume left is the pore space geometrically accessible from the outside by a spherical element with the value corresponding to the threshold value used.

This procedure can be used to detect the parts of the pore space theoretically accessible to microorganisms of known size, using only geometric parameters. This isolates the volumes of the samples accessible by the different structuring elements form the outside, along pathways with throats larger than the structuring element. Although this approximation is based solely on geometry, such calculations allow to obtain some information about which parts of the sample could be accessible to different classes of microorganisms, segmented by their characteristic size. Bearing in mind the resolution of the measurements, we considered three different classes of microorganisms based on their size: 0.65 μm for average microbial cells, 2 μm for large microbes, and 10 μm for protozoa. Aggregate microarchitecture can be expected to influence the distribution and

activity of microorganisms, for example microaggregates possessing large internal chambers with entrances small enough to selectively exclude larger competitors and/or predators would represent potential activity hotspots and refuges for select portions of the community. Results of the analysis are summarized again in Table 1. From this set of calculations, it is possible to see that both microaggregate samples are close to totally accessible to objects .65 μm large, while 2 μm structuring elements can still enter the majority of the pore-space in both the Barrow (86%) and Kansas (76%) samples. The largest (10 μm) structuring element, the size of small protozoa, cannot enter any of the pore space of the Kansas, inorganic-rich, microaggregate, while a small part of the sample (3%) is accessible in the Barrow one.

The potentially accessible parts of the pore space are displayed, superimposed to the 8bit volume rendering for all the particles in Figure 5. In this figure it is possible to observe the parts of the sample accessible to microbes of different sizes; for example the top lobe of the Kansas sample can be fully colonized by .65 μm microorganisms but has limited pore-space available to 2 μm microbes. Neither aggregate, with the exception of a single large pore in the Barrow sample, has a pores/throats system of sufficient size to accommodate 10 μm microorganisms, suggesting that both microaggregates could provide protection to internal communities from predation by protozoa. Previous microcosm studies have demonstrated that aggregate microstructure protects microbial communities from such predation (e.g., Vargas and Hattori, 1986, Wright et al. 1995) but prior studies could not characterize the internal aggregate structure which confers this effect.

*3.4 Skeleton analysis*

Another important descriptor of pore network topology is the pore space skeleton. A skeleton is a 1D topological descriptor of the 3D pore space which captures network connectivity in a simplified form, suitable for discrete models of flow and transport. In this study we used the "thinning" algorithm to efficiently compute the medial axes of both aggregate pore spaces (Lee et al., 1994; Lindquist et al., 1996; Palágyi and Kuba, 1999). The skeleton of the pore space of the connected network was calculated and the skeleton voxels were also labeled to identify branches, joints and end points in the framework.

The results of the skeleton analysis are summarized in Table 2. The network statistics indicates that the Barrow sample has the greater pore network complexity; this sample displays a significantly larger number of branches and junctions while the number of end points and the average branch length are very similar. This feature highlights a similar, basic, accessibility from the outside to two networks markedly different in complexity. This topic will be further analyzed and discussed, when another concept of "accessibility", based on the analysis of the size of the openings of the microaggregates facing the outside will be introduced. In Figure 4 a frequency distribution plot of the branch lengths in the two microaggregates is shown: the Barrow sample displays a wider distribution, with a larger number of the smallest and larger branch lengths, while the Kansas sample has a larger amount of the smaller (but not the smallest) branches. This, again, highlights the differences of the two pore network topologies, with the Barrow being the more complex.

The renderings of the two samples with the calculated thinning skeletons, labeled with respect to the LT value of each voxel to introduce pore diameter information in the skeleton, are shown in Figure 6. From the colors of the skeleton it is possible to see how in the Barrow sample the blue colors (extremely small values of LT) and the hotter colors (higher values of LT) are more frequent than in the Kansas sample, where small and moderately small (blue and greens) values are visibly more frequent. This is in accordance with the LT analysis discussed previously.

The network renderings also provide a qualitative representation of the differences in skeleton architecture between the two samples; the Kansas sample exhibits an interstitial skeleton, typical of the pore space generated from granular materials. In contrast, the Barrow sample shows more complicated structures, including components with many short branches and small LT values as well as parts with single long branches following the medial axes of the largest structures. These features appear to be generated by the interconnected cellular texture of the plant fragments incorporated into the aggregate.

*3.5 The interface to the outer world: openings analysis*

The outer surface of the aggregate is a critical interface linking it to the exterior environment, mediating gas and solute transport as well as microbial colonization. A key numerical task is, thus, extracting the apertures which exist on the aggregate exterior; these components are the required boundary condition for pore-scale modeling of diffusion and reaction within the single microaggregate system. As discussed in previous

sections, our processing flow has already extracted (a) the exterior bounding surface and (b) the skeleton and LT map for the aggregate pore space. By selecting the skeleton end-points which terminate within close proximity (5 voxel lengths) of the outer surface and then labeling them with the LT thickness we can generate a map of aggregate openings with the appropriate dimensions. The lower panel of figure 4 shows a histogram of the size of open pores on the aggregate surface for both samples considered. As can be seen, the slopes of the opening size distribution curves are markedly different, being the Barrow one steeper, highlighting a higher amount of small apertures, and a higher small-to-large apertures ratio. This is again a difference due to the Kansas being an aggregate of particles with an interstitial kind of pore space, while the Barrow is made of mainly small plant fragments with very small openings with a the few extremely large ones, where the biggest sects of the plant structure are broken and exposed to the surface. This results in the markedly different distribution of the openings.

Figure 7 provides a more graphical representation of the opening calculations showing grayscale volume renderings of the two microaggregates with opening pores marked in color. The paired figures show the same openings superimposed to the internal network structure (the skeleton in white). As can be seen, both samples are dominated by small exterior pores with the Barrow sample having smaller opening dimensions, indicated by the cooler colors (blue). The large exterior pores (orange/red) are relatively rare features on both aggregate surfaces.

*3.6 Anisotropy analysis*

Soil microaggregates can be formed by different components with varying shapes including rounded mineral particles, clay platelets, and fibrous/cellular organic materials as well as bioproducts. The shape of these constituent materials can control the shape of the microaggregate and the presence of anisotropic components can influence soil aggregate properties (e.g., Emerson, 1959). Considering that existing continuum models of gas diffusion in aggregates assume isotropic effective diffusivities, detection of strong pore-space anisotropy is a useful tool for evaluating the applicability of such models.

Fabric anisotropy can be measured directly from high quality tomographic datasets. One such approach is described in Voltolini et al. (2011), however it requires the separation of each single object in the dataset, a difficult constraint for aggregate characterization. When interior object separation is not possible, different approaches can be used. The most widely utilized technique is the mean intercept length (MIL) method (Withehouse, 1974), but this shows some limitations since it ideally requires spherical cropping and is prone to artifacts in datasets with objects described by small numbers of voxels. To minimize these issues we decided to use the star length distribution (SLD) method (Odgaard et al., 1997), which measures the mean object lengths for all orientations, using the implementation present in Quant3D (Ketcham and Ryan, 2004) for the first calculation, finally a series of Matlab® scripts based on the MTEX toolbox (Bachmann et al., 2010) were used for data handling, corrections, normalization and plotting.

To study the anisotropy of the two microaggregates we applied the SLD method to the solids and on the filled shape of the whole microaggregates. The former provides the quantification of the anisotropy of the internal migroaggregate structure (solids),

while the latter describes the anisotropy of the shape of the microaggregate itself. A comparison of the two pole figures (PFs) obtained from this analysis highlights any relationship of the microstructure with the shape of the microaggregate. In Figure 8 the PFs describing the Kansas and Barrow microaggregates for the solids and the whole microaggregates are plotted. In the Kansas sample (top) it can be seen that the structure is made by isotropic/randomly oriented components, since the PF displays values extremely close to one along all directions. Values in PFs are in multiples of random distribution (m.r.d.), where 1 is the value of a perfectly isotropic object and higher values towards $+\infty$ imply progressively stronger anisotropy. The orientation space with values <1 imply an orientation density smaller than a random (i.e. isotropic, uniform) distribution, and in addition to the maximum value, the minimum value in the PFs is an important parameter as well, representing the percentage of objects in the sample that can build a random distribution, thus giving additional information about the sharpness of the texture. The PF for the Kansas whole microaggregate denotes that some anisotropy is present; this is clearly visible from the renderings where the shape of the particle is elongated vertically and slightly flat, similarly to a 3-axes ellipsoid. This result shows that even if the microaggregate particle is elongated, there is no internal anisotropy present, in its components. This result is in line with the qualitative observation of the microaggregate constituents, where many rounded silt particles are recognizable.

The Barrow microaggregate is different; the PF of the whole particle suggests a slightly platy morphology, but the PF of the microstructure of the solids clearly shows a more fiber-like texture with the elongation axis in the platelet plane. The texture is weak (max at 1.25 m.r.d.), but anisotropy is clearly present. Relationships between PFs and the

sample can be seen at the bottom of Figure 8 where the renderings of the soil microaggregates, with the same orientation as the PFs are displayed. The virtual cut plane of the aggregates corresponds to the plane of the PFs as well. This analysis confirms that an accurate quantification of the anisotropy in single soil microaggregates is achievable using the methods described above.

***Discussion***

Two soil microaggregates of different origins and internal structures have been analyzed via sub-micron resolution SXR-μCT. A variety of techniques to analyze different microstructural parameters have been applied to provide a description of the different features of the aggregate microarchitecture in a descriptive fashion. This class of approaches are increasingly used in analysis of soil systems (e.g., De Gryze et al., 2006; Peth et al., 2008a,b; Zhou et al., 2013; Ma et al., 2015; Peth et al., 2015). The potential flexibility of the resolution/FOV ratio, with both conventional and unconventional X-ray sources, allows scans within a large range of scales (Sleutel et al., 2008). Synchrotron radiation, given its high flux, monochromaticity, and spatial coherence, has been recognized as a very important tool for the soil scientist since the first 3D imaging beamlines were developed (Spanne et al., 1994). Microtomographic data are also used for modeling more complex physical properties of soils and rocks, such as the Lattice Boltzmann approach for evaluating permeability (Menon et al., 2011; Khan et al., 2012) or direct numerical simulations of pore-scale reactive chemistry (Molins et al. 2012).

In this work we focus mainly on the geometrical differences of single microaggregates and exploit the high flux and resolution of BL 8.3.2 to provide a more detailed structural description. The new tools make it possible to develop the analysis of the entirety of microaggregates at sub-micron resolution, overcoming the need to crop subvolumes. This is of great importance since we were able to study the interface of the single microaggregates with the external world, whereas cropped volumes would make this kind of study impossible, and would not provide correct boundary conditions when used for modeling.

The size of the two microaggregate studied is similar. From the analysis of the internal porosity, it is clear that the microaggregate richer in organic matter (Barrow) is about twice as porous as the predominantly inorganic one (Kansas). This increased porosity appears to be the result of large pores with a cellular texture, as visible in Figure 2b. While a statistically valid generalization from our small sample set is not possible, the results from the Barrow aggregate suggest that detrital plant matter has an important role in controlling internal porosity. Prior studies of microaggregate structure have noted that formation often initiates around a "core" of plant debris (Oades and Waters 1991, Golchin et al. 1994); our results suggest that this core material may also provide a unique structural environment for microbial activity distinct from microaggregates which are primarily granular in texture. It is important to remark that in this work we are only comparing two aggregates with different texture and composition to find the morphometric parameters that would better describe those differences, and the links of those parameters with specific properties of the aggregate; we are not comparing two specific environments. The latter task would require a much larger number of samples,

and likely a different approach, combining multi-resolution measurements, where the large FOV would be used to identify the different type/classes of microaggregates present in each locale (and quantify their distribution), while the high resolution would target the specific single microaggregates (as shown in this work), representative for each class, to fully characterize them. Such an approach would likely allow reaching an acceptable statistical meaningfulness for each site, as needed to take into account some of the intra-site variability of microaggregates, but without measuring an unrealistically high number of single microaggregates and run a full analysis on all of them.

The internal aggregate surface area is another important parameter due to both its role in reaction kinetics as well as a microbial growth substrate. Concerning the surface area of the two microaggregates, the Barrow sample shows a larger surface area with a slightly higher complexity than the Kansas sample. This is likely due to the rough surface present in the Kansas sample, composed mainly of poorly sorted silt/clay particles, and the smoother surfaces present in the Barrow sample. However, the complexity of the pores space in the Barrow sample ultimately generates a higher surface area per volume.

The Minkowski functionals, as expected, describe a complex structure with a tightly interconnected pore space. This is also confirmed by the skeleton analysis, highlighting again the extensive complexity of the soil microaggregates at this scale. The fractal analysis shows a moderate fractal behavior for both the microaggregates, with no significant differences between the inorganic- and organic- based particles. Independent of use as a complexity measure, the fractal dimension of aggregates has been linked to measures of erodability in past studies (e.g., Ahmadi et al. 2011), hence it may such measurements may provide insight to microaggregate evolution over time.

The LT analysis discussed previously provides detailed information on pore space statistics across the aggregate; the distribution of voxel LT values provides useful statistical constraints including the aperture variance, a key parameter in stochastic network models of soil structure which is often guessed at. The LT distribution in the Kansas sample is clearly sharper than the Barrow aggregate, which exhibits a higher variance in pore sizes and apertures. This statistical difference is due to the plant fragments: the large voids present in these structures, coupled with small voids generated by clay particle aggregation, generated a broader distribution of pores. These observations suggest that the Barrow microaggregate might provide a better host for microbial activity due to the combination of a large internal porosity and a broad size distribution of internal microenvironments.

The novel strategy for soil particles analysis presented also allows the calculation of pore space accessibility metrics for single aggregates, potentially a key control on protection of aggregate microbial communities from predation by larger organisms (e.g., protozoa). It is worth remarking that this is a theoretical accessibility based purely on the geometry of the pore space: features such as characteristic microorganism shape, biological needs, reproduction rates, etc. are not considered. The resulting accessibility metrics assume a rigid spherical body to determine the ideal potential access. We have chosen three different sizes, compatible with characteristic organism sizes and image resolution. First we have performed the accessibility analysis for objects .65 μm large, a typical mid-size bacterial cell. The theoretical accessibility for a virtual microorganism of this size from outside the sample is very large: 95% for the Kansas sample and 98% for the Barrow aggregate. This is not surprising since this value is close to the resolution of

the measurement and the pore space is strongly interconnected. More interesting is the accessibility for objects with the size comparable to large bacteria strains: 2 μm. The differences here are more marked since some parts of the Kansas sample, more complex and with small, not well connected, pores are present and therefore they are non-accessible to the 2 μm virtual bacteria. In the Barrow sample the accessibility is still very high (86%, compared with the 76% of Kansas), this is due to the fact that the size of the object is still smaller than the size of a significant number of openings on the surface and because of the very high connectivity (and throat sizes) of the pore space, allowing the objects to move rather freely once entered the microaggregate pore space.

As a last test, we considered objects 10 μm large: this is the size of small protozoa, an active bacterial predator. Prior experimental studies (Wright et al. 1995) have utilized even larger protozoa with mean sizes in the 20-30 μm range (*C. steinii)* to study the protective nature of aggregates. A microaggregate largely accessible to protozoa would be potentially unsafe for the internal microbial community. In the two microaggregates examined, the virtual protozoa cannot enter any pore space in the Kansas sample, and can only enter a small single portion of the pore space in the Barrow one, highlighting how these microaggregates can in theory provide a protective environment for bacterial communities. Our imaging study is largely consistent with prior experiments documenting this phenomenon (Vargas and Hattori, 1986, Wright et al. 1995). Given the protective role of microaggregates and the availability of a diverse set of associated microenvironments (Ranjard and Richaume, 2001), the role of aggregate pore morphology in controlling community structure might provide a promising path

towards understanding the biogeochemical response of such systems (Remenant et al. 2009).

In addition to bulk accessibility metrics, we quantified the aperture dimensions of the outer surface of each aggregate sample, a metric useful in defining outer boundary conditions and flux limitations for gas transport. In the Kansas sample the exterior aperture sizes are generally larger than the Barrow sample as can be seen in the color map used in Figure 7. The Barrow sample does however have a small number of large open exterior pores generated by open tubular structures present in the detrital plant components. This analysis provides a quantitative approach to estimating the unoccluded surface/total volume ratio for the aggregate, a parameter required when modeling oxygen diffusion and consumption in aggregated soils (e.g., Renault and Stengel, 1994).

The analysis of anisotropy revealed that the Kansas aggregate is effectively isotropic in terms of microstructure despite an elongated shape. In contrast, the Barrow aggregate was anisotropic on the pore scale due to the presence of aligned pores in the detrital plant fragment. While we did not numerically compute effective diffusivity coefficients for the two aggregate samples, the lower isotropy index for the Barrow sample (0.763) suggest that preferential diffusion along the axis of the aligned pores could significantly impact gas and solute transport.

Figure 9 provides a graphical summary of the analysis suite displayed for a thin (~20 μm) horizontal slice in each aggregate. Each image shows the typical characteristics discussed in this section and it is possible to better understand the differences in LT, skeleton and openings in the two microaggregates. In Figure 9a the 8bit rendering of the solids is superimposed with the LT volume: the differences in porosity and pore size

distributions are immediately visible, as in Figure 9b (LT volume alone). In Figure 9c the 8bit volume is superimposed with the skeleton (labeled with the LT values) and the openings (labeled with a color corresponding to their diameter). It is possible to appreciate how well the skeleton fits the pore space and the role of the bigger chambers due to the presence of the plant fragments in the Barrow microaggregate. In Figure 9d the 8-bit volume is removed to highlight the features of the skeletons and of the openings; we see a more complex pattern of the skeleton in the barrow samples with shorter and smaller branching linking the outside of the particle with the pore space, while the Kansas particle displays classic interstitial pore space features in both the skeleton and the openings.

A significant potential use of the detailed structural analysis presented is for the direct numerical modeling of pore-scale biogeochemical processes in microaggregates. The recent study of Ebrahimi and Or (2015) presents an elegant network modeling approach capable of capturing the boundary of aerobic activity and community partitioning within a single aggregate. The network architecture used in the modeling, however, was a theoretical regular framework generated to match capillary pressure/matric potential data on an aggregate collection and did not contain the detail present in our direct imaging study. We believe that high quality SXR-μCT can fill an important gap in such modeling studies by providing an appropriate network, aperture distribution, and set of boundary conditions to realistically capture biogeochemical processes at the aggregate scale. This interaction between experimentalists providing the modelers realistic starting points and validation datasets is bound to become more and more important in many fields. The new direction of building online experimental data

repositories (e.g., https://www.digitalrocksportal.org/) will also have an increasingly important role in connecting experimental and modeling groups, including of course the soil scientist community.

## *Conclusions*

SXR-μCT measurements on single soil microaggregates, coupled with advanced analysis techniques have significant potential to improve the characterization of this unique microbial environment. The suite of tools we present may aid future studies seeking to correlate aggregate microstructure with microbial community structure and function. In this study two markedly different microaggregates have been analyzed and the results show how soil microstructures can be quantified and potentially linked back to biological processes. Prior work has demonstrated a direct impact for different processes such as the protection from predators (Griffiths and Young, 1994; Young and Ritz, 1998), the distribution of nutrients (Chenu et al., 2001), or for environmental issues such as local variations in heavy metal concentrations (Ranjard et al., 2000).

In the two samples we have shown the Kansas microaggregate, mostly inorganic in nature, displays a typical interstitial pore space, created by the aggregation of rounded mineral particles and aggregates. A more complex microstructure is present in the Barrow microaggregate, with a strong organic component, discernible also from the XR attenuation values, due to the high percentage of plant fragments. This microaggregate shows a significantly larger amount of pore space potentially available to bacteria, and

this pore space is accessible only to small- to medium- sized microorganisms. Following the geometrical concept alone the Barrow microaggregate provides a better environment for the potential development of bacteria colonies, providing a larger and well protected space to the microorganisms.

The quantitative microstructural characterization -aim of the present work- albeit fundamental, is only a single element for a truly complete characterization of soil microaggregates. The distribution of the chemical compounds needed for the development of the microorganisms, and of microorganisms themselves, in the microaggregates also play a key role and a comprehensive study about the role of microaggregates in the development of spots of highly increased biological activity in soils. Future improvements in X-ray imaging techniques, with both conventional and unconventional sources, and further improvements and automation of the analysis part will play an important role in achieving a better knowledge of the mechanisms related to soil microaggregates, especially when coupled with techniques aimed at describing the distribution of the different microbial communities.

***Acknowledgement***

The authors acknowledge the Advanced Light Source staff at BL 8.3.2. Dula Parkinson and Alastair MacDowell for the help with the beamline setup. The Advanced Light Source is supported by the Director, Office of Science, Office of Basic Energy Sciences, of the U.S. Department of Energy under Contract No. DE-AC02-05CH11231. This work has been founded through the Lawrence Berkeley National Laboratory Directed Research

and Development (LDRD) "Integrative mapping of soil heterogeneity at the microbial scale" #366197. We thank an anonymous reviewer whose comments helped to improve and clarify this manuscript.

***References***

Accardo, A.P., Strolka, I., Toffanin, R., Vittur, F., 2005. Medical imaging analysis of the three dimensional (3D) architecture of trabecular bone: techniques and their applications. Medical Imaging Systems Technology-Methods in General Anatomy. Singapura: World Scientific Publishing Co. Pte. Ltd, 1-41.

Anderson, S.H., Peyton, R.L., Gantzer, C. J., 1990. Evaluation of constructed and natural soil macropores using X-ray computed tomography. Geoderma, 46(1), 13-29.

Anderson, A.N., Mcbratney, A.B., 1995. Soil aggregates as mass fractals. Aus. J. Soil Res. 33(5), 757-772.

Arzilli, F., Mancini, L., Voltolini, M., Cicconi, M.R., Mohammadi, S., Giuli, G., Mainprice, D., Paris, E., Barou, F. and Carroll, M.R., 2015. Near-liquidus growth of feldspar spherulites in trachytic melts: 3D morphologies and implications in crystallization mechanisms. Lithos, 216, 93-105.

Bachmann, F., Hielscher, R., Schaeben, H., 2010. Texture analysis with MTEX–free and open source software toolbox. Sol. St. Phen., 160, 63-68.

Bailey, V.L., McCue, L.A., Fansler, S.J., Boyanov, M.I., DeCarlo, F., Kemner, K.M. Konopka, A., 2013. Micrometer-scale physical structure and microbial composition of soil macroaggregates. Soil Biol. Biochem., 65, pp.60-68.

Bronnikov, A.V., 2002. Theory of quantitative phase-contrast computed tomography. JOSA A, 19(3), 472-480.

Bundt, M., Widmer, F., Pesaro, M., Zeyer, J., Blaser, P., 2001. Preferential flow paths: biological 'hot spots' in soils. Soil Biol. Biochem., 33(6), 729-738.

Chenu, C., Hassink, J., Bloem, J., 2001. Short-term changes in the spatial distribution of microorganisms in soil aggregates as affected by glucose addition. Biol. Fert. Soils, 34(5), 349-356.

Chenu, C., Stotzky, G., 2002. Interactions between microorganisms and soil particles: an overview. Interactions between soil particles and microorganisms: Impact on the terrestrial ecosystem. IUPAC. John Wiley and Sons, Ltd., Manchester, UK, pp.1-40.

Clausnitzer, V., Hopmans, J.W., 1999. Determination of phase-volume fractions from tomographic measurements in two-phase systems. Adv. Water Resour., 22(6), 577-584.

Currie, J.A., 1962. The importance of aeration in providing the right conditions for plant growth. J. Sci. Food. Agric., 13, pp. 380-385.

De Gryze, S., Jassogne, L., Six, J., Bossuyt, H., Wevers, M., Merckx, R., 2006. Pore structure changes during decomposition of fresh residue: X-ray tomography analyses. Geoderma, 134(1), 82-96.

Dougherty, R., Kunzelmann, K. H., 2007. Computing local thickness of 3D structures with ImageJ. Microsc. Microanal., 13(S02), 1678-1679.

Ebrahimi, A., Or, D., 2015. Hydration and diffusion processes shape microbial community organization and function in model soil aggregates. Water Resour. Res., 51, pp. 9804-9827.

Edwards, A. P., Bremner, J. M., 1967. Microaggragates in soils. J. Soil Sc., 18(1), 64-73.

Emerson, W.W., 1959. Stability of soil crumbs. Nature, 138, 538-538.

Foster, R.C., 1988. Microenvironments of soil microorganisms. Biol. Fert. Soils, 6(3), pp.189-203.

Gibson, J. R., Lin, H., Bruns, M. A., 2006. A comparison of fractal analytical methods on 2-and 3-dimensional computed tomographic scans of soil aggregates. Geoderma, 134(3), 335-348.

Gimenez, D., Perfect, E., Rawls, W. J., Pachepsky, Y., 1997. Fractal models for predicting soil hydraulic properties: a review. Eng. Geol., 48(3), 161-183.

Griffiths, R. S., and Young, I. M. 1994. The effects of soil structure on protozoa in a clay -loam soil. Eur. J. Soil Sc., 45(3), 285-292.

Heeraman, D. A., Hopmans, J. W., Clausnitzer, V., 1997. Three dimensional imaging of plant roots in situ with X-ray computed tomography. Plant Soil, 189(2), 167-179.

Heijs, A. W., De Lange, J., Schoute, J. F., Bouma, J., 1995. Computed tomography as a tool for non-destructive analysis of flow patterns in macroporous clay soils. Geoderma, 64(3), 183-196.

Hu, Q., Qian, G., Nowinski, W. L., 2005. Fast connected-component labelling in three-dimensional binary images based on iterative recursion. Comput. Vis. Image Und., 99(3), 414-434.

Kak, A.C., Slaney, M., 1987. Principles of Computerized Tomography, New York, IEEE Press.

Ketcham, R.A., Ryan, T.M., 2004. Quantification and visualization of anisotropy in trabecular bone. J. Microsc., 213(2), 158-171.

Khan, F., Enzmann, F., Kersten, M., Wiegmann, A., Steiner, K., 2012. 3D simulation of the permeability tensor in a soil aggregate on basis of nanotomographic imaging and LBE solver. J. Soils Sedim., 12(1), 86-96.

Lee, T.C., Kashyap, R.L., Chu, C.N., 1994. Building skeleton models via 3-D medial surface axis thinning algorithms. CVGIP: Graph. Model. Im. Proc., 56(6), 462-478.

Liebovitch, L.S., Toth, T., 1989. A fast algorithm to determine fractal dimensions by box counting. Phys. Lett. A, 141(8), 386-390.

Lindquist, W.B., Lee, S.M., Coker, D.A., Jones, K.W., Spanne, P., 1996. Medial axis analysis of void structure in three-dimensional tomographic images of porous media. J. Geophy. Res.-Sol. Ea. (1978–2012), 101(B4), 8297-8310.

Ma, R., Cai, C., Li, Z., Wang, J., Xiao, T., Peng, G., Yang, W., 2015. Evaluation of soil aggregate microstructure and stability under wetting and drying cycles in two Ultisols using synchrotron-based X-ray micro-computed tomography. Soil Till. Res., 149, 1-11.

Macedo, A., Crestana, S., Vaz, C.M.P., 1998. X-ray microtomography to investigate thin layers of soil clod. Soil Till. Res., 49(3), 249-253.

Menon, M., Yuan, Q., Jia, X., Dougill, A.J., Hoon, S.R., Thomas, A.D., Williams, R.A., 2011. Assessment of physical and hydrological properties of biological soil crusts using X-ray microtomography and modeling. J. Hydrol., 397(1), 47-54.

McBratney, A.B., 1993. Comments on "Fractal Dimensions of Soil Aggregate-Size Distributions Calculated by Number and Mass". Soil Sci. Soc. Am. J., 57(5), 1393-1393.

McCarthy, J.F., Ilavsky, J., Jastrow, J.D., Mayer, L.M., Perfect, E. Zhuang, J., 2008. Protection of organic carbon in soil microaggregates via restructuring of aggregate porosity and filling of pores with accumulating organic matter. Geochim. Cosmochim. Ac., 72(19), pp.4725-4744.

Molins, S., Trebotich, D., Steefel, C.I., Shen, C., 2012. An investigation of the effect of pore scale flow on average geochemical reaction rates using direct numerical simulation. Water Resour. Res. 48(W03527).

Mooney, S.J., Pridmore, T.P., Helliwell, J., Bennett, M.J., 2012. Developing X-ray Computed Tomography to non-invasively image 3-D root systems architecture in soil. Plant Soil, 352(1-2), 1-22.

Nunan, N., Ritz, K., Rivers, M., Feeney, D.S., Young, I.M., 2006. Investigating microbial micro-habitat structure using X-ray computed tomography. Geoderma, 133(3), 398-407.

Oades, J.M., 1984. Soil organic matter and structural stability: mechanisms and implications for management. Plant Soil, 76(1-3), 319-337.

Odgaard, A., 1997. Three-dimensional methods for quantification of cancellous bone architecture. Bone, 20(4), 315-328.

Odgaard, A., Kabel, J., van Rietbergen, B., Dalstra, M., Huiskes, R., 1997. Fabric and elastic principal directions of cancellous bone are closely related. J. Biomech., 30(5), 487-495.

Ohser, J., Mücklich, F., 2000. Statistical analysis of microstructures in materials science. Chichester: Wiley.

Or, D., Smets, B.F., Wraith, J.M., Dechesne, A., Friedman, S.P., 2007. Physical constraints affecting bacterial habitats and activity in unsaturated porous media–a review. Adv. Water Resour., 30(6), pp.1505-1527.

Paganin, D., Mayo, S.C., Gureyev, T.E., Miller, P.R., Wilkins, S.W., 2002. Simultaneous phase and amplitude extraction from a single defocused image of a homogeneous object. J. Microsc., 206(1), 33-40.

Palágyi, K., Kuba, A., 1999. A parallel 3D 12-subiteration thinning algorithm. Graph. Model Im. Proc., 61(4), 199-221.

Parfitt, A.M., Drezner, M.K., Glorieux, F.H., Kanis, J.A., Malluche, H., Meunier, P.J., Ott, S.M., Recker, R.R., 1987. Bone histomorphometry: standardization of nomenclature, symbols, and units: report of the ASBMR Histomorphometry Nomenclature Committee. J. Bone Miner. Res., 2(6), 595-610.

Perfect, E., Rasiah, V., Kay, B.D., 1992. Fractal dimensions of soil aggregate-size distributions calculated by number and mass. Soil Sc. Soc. Am. J., 56(5), 1407-1409.

Peth, S., Horn, R., Beckmann, F., Donath, T., Smucker, A.J., 2008, August. The interior of soil aggregates investigated by synchrotron-radiation-based microtomography. In Optical Engineering+ Applications (pp. 70781H-70781H). International Society for Optics and Photonics.

Peth, S., Horn, R., Beckmann, F., Donath, T., Fischer, J., Smucker, A.J. M., 2008. Three-dimensional quantification of intra-aggregate pore-space features using synchrotron-radiation-based microtomography. Soil Sc. Soc. Am. J., 72(4), 897-907.

Peth, S., Chenu, C., Leblond, N., Mordhorst, A., Garnier, P., Nunan, N., Pot, V., Ogurreck, M., Beckmann, F., 2014. Localization of soil organic matter in soil aggregates using synchrotron-based X-ray microtomography. Soil Biol. and Biochem., 78, pp.189-194.

Petrovic, A.M., Siebert, J.E., Rieke, P.E., 1982. Soil bulk density analysis in three dimensions by computed tomographic scanning. Soil Sci. Soc. Am. J., 46(3), 445-450.

Peyton, R.L., Haeffner, B.A., Anderson, S.H., Gantzer, C.J., 1992. Applying X-ray CT to measure macropore diameters in undisturbed soil cores. Geoderma, 53(3), 329-340.

Peyton, R.L., Gantzer, C.J., Anderson, S.H., Haeffner, B.A., Pfeifer, P., 1994. Fractal dimension to describe soil macropore structure using X ray computed tomography. Water Resour. Res., 30(3), 691-700.

Phillips, J.D., 2009. Soils as extended composite phenotypes. Geoderma, 149(1), pp.143-151.

Pierret, A., Capowiez, Y., Belzunces, L., Moran, C. J., 2002. 3D reconstruction and quantification of macropores using X-ray computed tomography and image analysis. Geoderma, 106(3), 247-271.

Ranjard, L., Nazaret, S., Gourbière, F., Thioulouse, J., Linet, P., Richaume, A., 2000. A soil microscale study to reveal the heterogeneity of Hg (II) impact on indigenous bacteria by quantification of adapted phenotypes and analysis of community DNA fingerprints. FEMS Microbiol. Ecol., 31(2), 107-115.

Remenant, B., Grundmann, G.L., L. Jocteur-Monrozier., 2009. From the micro-scale to the habitat: Assessment of soil bacterial community structure as shown by soil structure directed sampling, Soil Biol. Biochem., 41, pp. 29-36.

Renault, P., Stengel, P., 1994. Modeling Oxygen Diffusion in Aggregated Soils: I. Anaerobiosis inside the Aggregates, Soil Sci. Soc. Am. J., 58, pp. 1017-1023.

Russ, J. C., DeHoff, R. T. 2012 Practical stereology. Springer Science & Business Media.

Schindelin, J., Arganda-Carreras, I., Frise, E., Kaynig, V., Longair, M., Pietzsch, T., Cardona, A. 2012. Fiji: an open-source platform for biological-image analysis. Nature Methods, 9(7), 676-682.

Silin, D., Tomutsa, L., Benson, S.M., Patzek, T.W. 2010 Microtomography and pore-scale modeling of two-phase fluid distribution. Transport Porous Med., 86(2), 495-515.

Simmons, C.A., Hipp, J.A., 1997. Method-based differences in the automated analysis of the three-dimensional morphology of trabecular bone. J. Bone Miner. Res., 12(6), 942-947.

Six, J., Paustian, K., Elliott, E.T., Combrink, C., 2000. Soil structure and organic matter I. Distribution of aggregate-size classes and aggregate-associated carbon. Soil Sci. Soc. Am. J., 64(2), 681-689.

Six, J.A.E.T., Elliott, E.T., Paustian, K., 2000. Soil macroaggregate turnover and microaggregate formation: a mechanism for C sequestration under no-tillage agriculture. Soil Biol. Biochem., 32(14), pp.2099-2103.

Six, J., Bossuyt, H., Degryze, S., Denef, K., 2004. A history of research on the link between (micro) aggregates, soil biota, and soil organic matter dynamics. Soil Till. Res., 79(1), 7-31.

Sleutel, S., Cnudde, V., Masschaele, B., Vlassenbroek, J., Dierick, M., Van Hoorebeke, L., De Neve, S., 2008. Comparison of different nano-and micro-focus X-ray computed tomography set-ups for the visualization of the soil microstructure and soil organic matter. Comput. Geosci., 34(8), 931-938.

Smith, K.A., 1980. A model of the extent of anaerobic zones in aggregates soils, and its potential application to estimates of denitrification. J. Soil Sci., 31, pp. 263-277.

Spanne, P., Jones, K.W., Prunty, L., Anderson, S.H., 1994. Potential applications of synchrotron computed microtomography to soil science. Tomography of Soil-Water-Root Processes (Conference Proceedings), 43-57.

Tisdall, J.M., Oades, J., 1982. Organic matter and water-stable aggregates in soils. J. Soil Sci., 33(2), 141-163.

Vargas, R., Hattori, T., 1986. Protozoan predation of bacterial cells in soil aggregates. FEMS Microbiol. Ecol., 38, pp. 233-242.

Vogel, C., Mueller, C.W., Höschen, C., Buegger, F., Heister, K., Schulz, S., Schloter, M., Kögel-Knabner, I., 2014. Submicron structures provide preferential spots for carbon and nitrogen sequestration in soils. Nature Comm., 5.

Voltolini, M., Zandomeneghi, D., Mancini, L., Polacci, M., 2011. Texture analysis of volcanic rock samples: Quantitative study of crystals and vesicles shape preferred orientation from X-ray microtomography data. J. Volcanol. Geoth. Res., 202(1), 83-95.

Weitkamp, T., Haas, D., Wegrzynek, D., Rack, A., 2011. ANKAphase: software for single-distance phase retrieval from inline X-ray phase-contrast radiographs. J. Synchrotron Radiat., 18(4), 617-629.

Whitehouse, W.J., 1974. The quantitative morphology of anisotropic trabecular bone. J. Microsc., 101(2), 153-168.

Wright, D.A., Killham, K., Glover, L.A., Prosser, J.I., 1995. Role of Pore Size Location in Determining Bacterial Activity during Predation by Protozoa in Soil. Appl. Environ. Microbiol., 61(10), 3537-3543.

Young, I. M., Ritz, K., 1998. Can there be a contemporary ecological dimension to soil biology without a habitat? Soil Biol. Biochem., 30(10-11), 1229-1232.

Young, I.M., Crawford, J.W., 1991. The fractal structure of soil aggregates: its measurement and interpretation, J. Soil Sci., 42, 187-192.

Young, I.M., Crawford, J.W., 2004. Interactions and self-organization in the soil-microbe complex. Science, 304(5677), 1634-1637.

Yushkevich, P.A., Piven, J., Hazlett, H.C., Smith, R.G., Ho, S., Gee, J.C., Gerig, G., 2006. User-guided 3D active contour segmentation of anatomical structures: significantly improved efficiency and reliability. Neuroimage, 31(3), 1116-1128.

Zhou, H., Peng, X., Perfect, E., Xiao, T., Peng, G., 2013. Effects of organic and inorganic fertilization on soil aggregation in an Ultisol as characterized by synchrotron based X-ray micro-computed tomography. Geoderma, 195, 23-30.

***Figure Captions***

Figure 1.

Whole and vertically cut volume renderings of the Kansas and Barrow soil microaggregates.

Figure 2.

Barrow microaggregate showing the calculated "outer surface" (displayed in red), in a vertically cut sample with a partial covering of the surface (a), and a thin slice with the surface following the outer border (b).

Figure 3.

The two microaggregates showing the local thickness volume superimposed to the 8bit volume rendering and alone. Volumes are cut to better show the internal features.

Figure 4.

Frequency plots showing the distribution of (from top to bottom): local thickness voxels, skeleton branch lengths, surface openings.

Figure 5.

Pore space accessibility from the outside for spherical structuring elements of different sizes: .65 μm (yellow), 2 μm (green), 10 μm (red).

Figure 6.

Renderings of the skeletons, displayed superimposed both with a cut 8bit volume and alone. The skeleton is labeled with the local thickness values for each voxel.

Figure 7.

Analysis of openings: the rendering on the left for the two microaggregates shows the 8bit rendering with the openings marked bi cubes labeled with respect their size. On the right the skeleton and the openings alone are plotted.

Figure 8.

Star Length Distribution analysis for anisotropy characterization. The SLD analysis has been carried out on both the solids of the microaggregates (PF's on the left) and the whole completely filled aggregate (PF's on the right). Values are in multiples of random distribution, PF's are in equal area projection, upper hemisphere. The bottom of the figure shows the whole and horizontally sectioned microaggregates oriented as the PF's.

Figure 9.

Thin horizontal slice of the two samples showing in more details and summarizing the main analyses carried out on the microaggregates.

Table 1. Morphometric analysis.

| | ***Kansas*** | ***Barrow*** |
|---|---|---|
| *Volumetric Analysis* | | |
| Total Aggregate Volume [$\mu m^3$] | 2.819E+06 | 3.619E+06 |
| Total Volume of solids [$\mu m^3$] | 1.970E+06 | 1.998E+06 |
| Total Volume of voids [$\mu m^3$] | 8.486E+05 | 1.621E+06 |
| Porosity [%] | 43.1 | 81.1 |
| *Surface Area Analysis* | | |
| Surface Area [$\mu m^2$] | 3.505E+06 | 4.850E+06 |
| SNSVR | 11.8 | 13.8 |
| *Minkowski Functionals and Fractal Analysis* | | |
| Integral of mean curvature (solids) [$\mu m^{-2}$] | -45197.6 | -21798.8 |
| Euler Characteristic (voids) [$\mu m^{-3}$] | -312.6 | -410.6 |
| Fractal dimension 3D (voids) | 2.353 | 2.401 |
| *Local Thickness Analysis* | | |
| Structure Separation Mean [μm] | 3.13 | 5.32 |
| Structure Separation σ [μm] | 1.89 | 4.13 |
| Structure Separation Max [μm] | 12.77 | 24.74 |
| Structure Thickness Mean [μm] | 6.46 | 7.45 |
| Structure Thickness σ [μm] | 5.44 | 11.44 |
| Structure Thickness Max [μm] | 28.66 | 47.07 |
| *Geometrical Accessibility Analysis* | | |
| 0.65 μm elements accessibility [% of voids] | 95.5 | 98.0 |
| 2 μm elements accessibility [% of voids] | 76.0 | 86.2 |
| 10 μm elements accessibility [% of voids] | 0 | 3.2 |
| *Anisotropy analysis SLD -solids-* | | |
| Isotropy index (I) | 0.937 | 0.763 |
| Elongation index (E) | 0.019 | 0.153 |

Table 2. Skeleton analysis

| | ***Kansas*** | ***Barrow*** |
|---|---|---|
| Number of branches | 54550 | 81012 |
| Number of true junctions | 29752 | 44202 |
| Number of end points | 11143 | 13552 |
| Number of triple points | 23113 | 33105 |
| Number of quadruple points | 4953 | 7713 |
| Average branch length [μm] | 3.41 | 3.40 |

| | | |
|---|---|---|
| Max branch length [μm] | 24.54 | 46.07 |

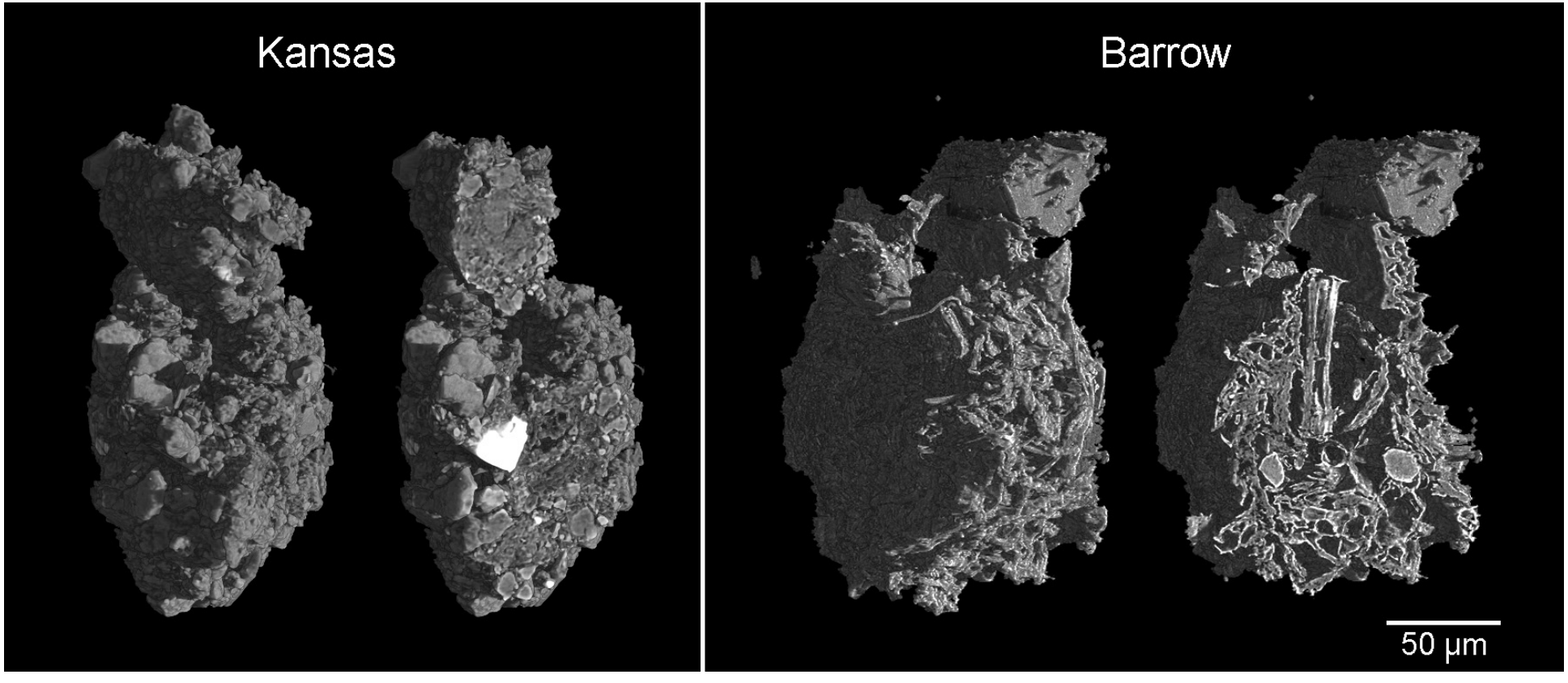
Kansas
Barrow
50 µm

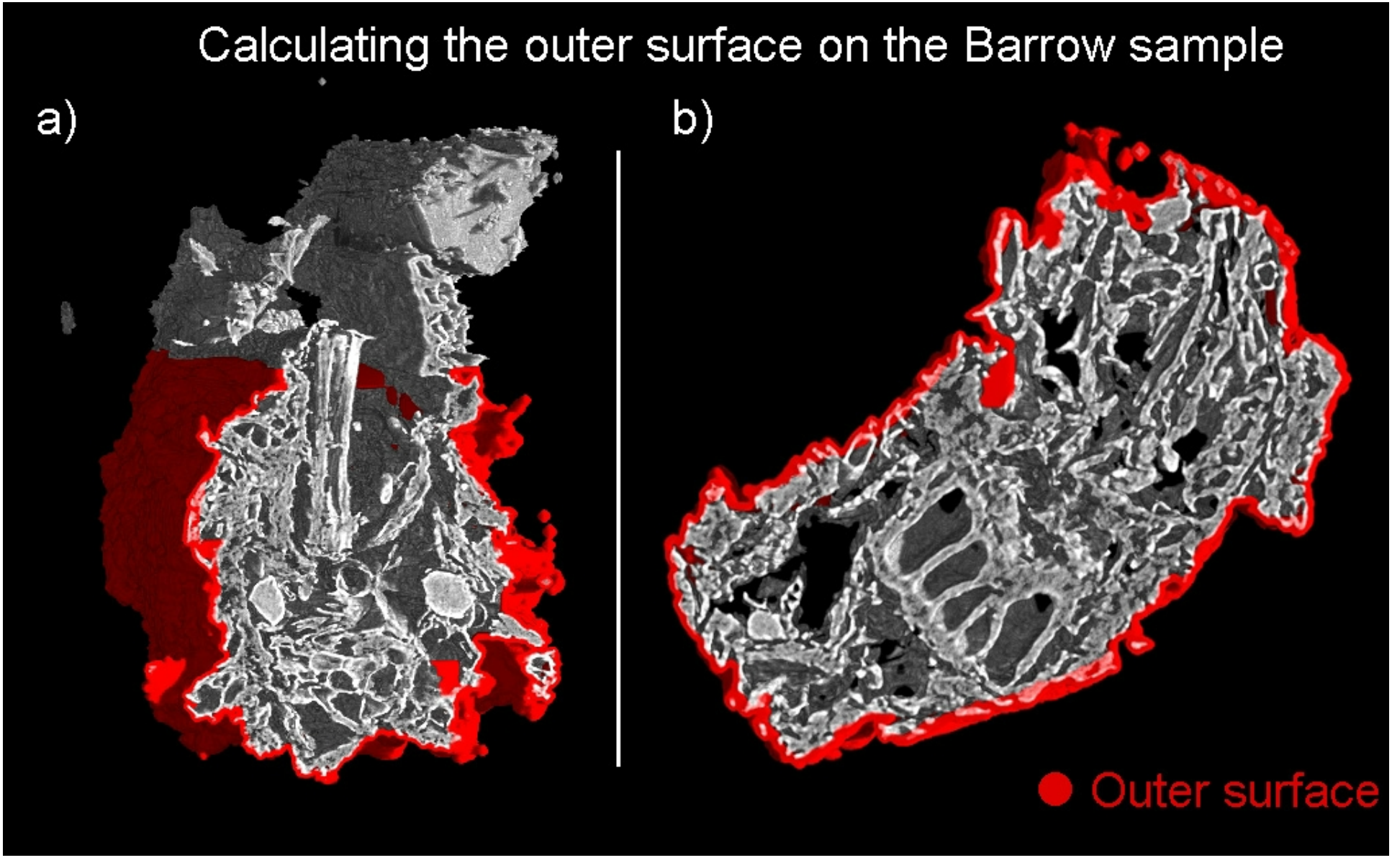
Calculating the outer surface on the Barrow sample
a)
b)
Outer surface

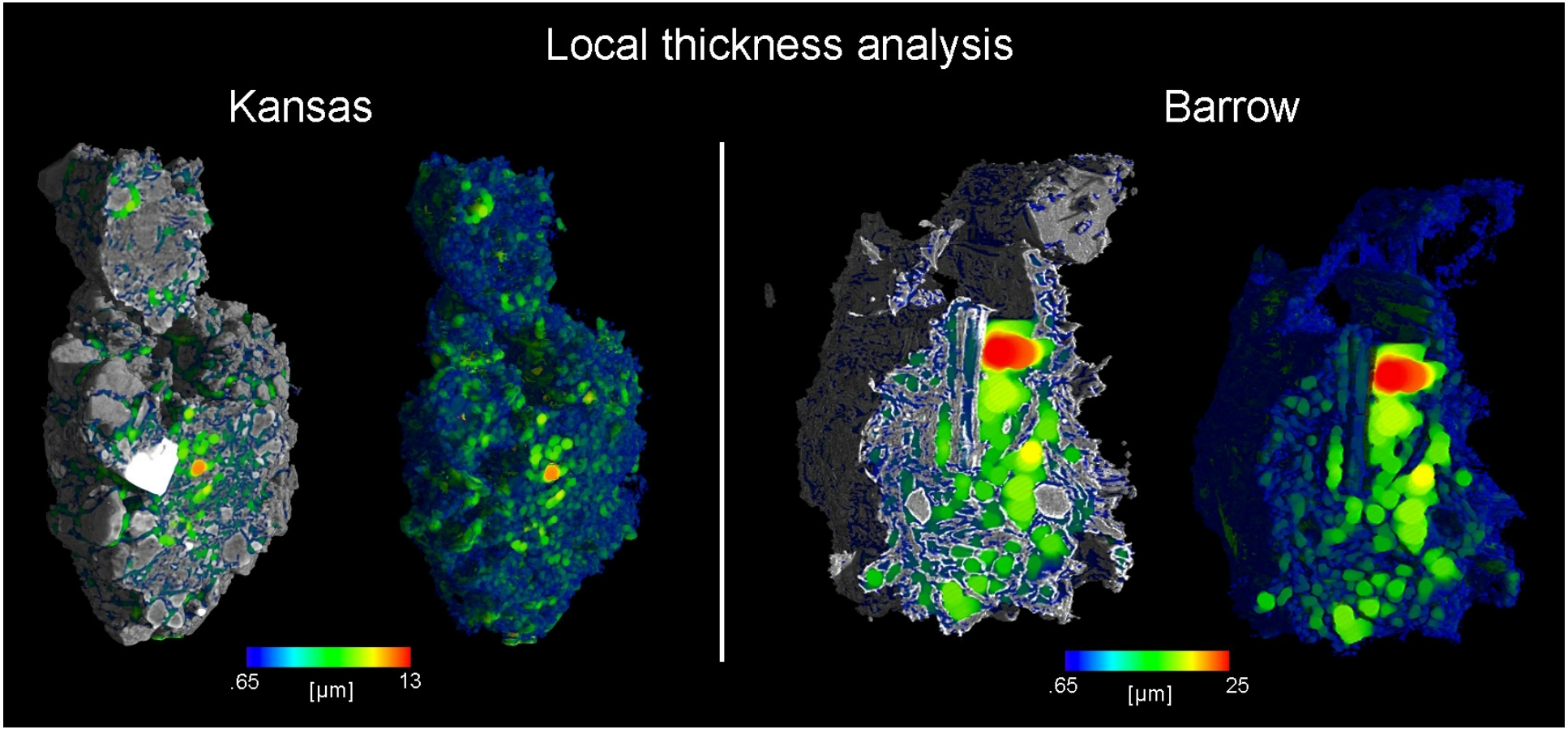
Local thickness analysis
Kansas
Barrow
.65
[µm]
13
.65
[µm]
25

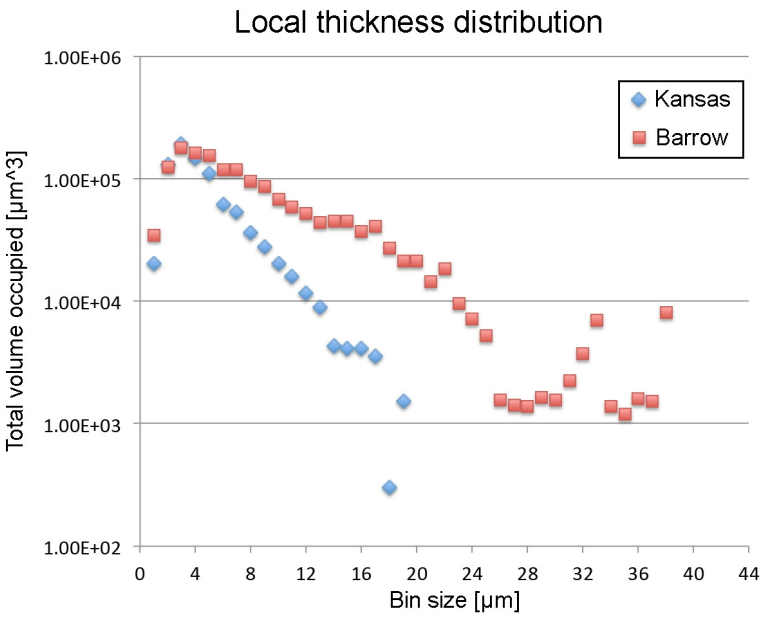
Local thickness distribution
Kansas
Barrow
Total volume occupied [µm^3]
1.00E+06
1.00E+05
1.00E+04
1.00E+03
1.00E+02
0
4
8
12
16
20
24
28
32
36
40
44
Bin size [µm]

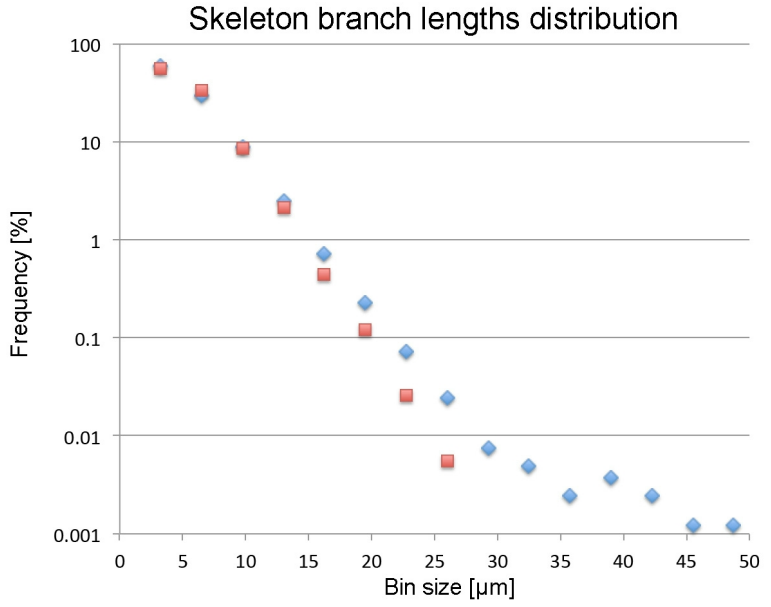
Skeleton branch lengths distribution
Frequency [%]
100
10
1
0.1
0.01
0.001
0
5
10
15
20
25
30
35
40
45
50
Bin size [µm]

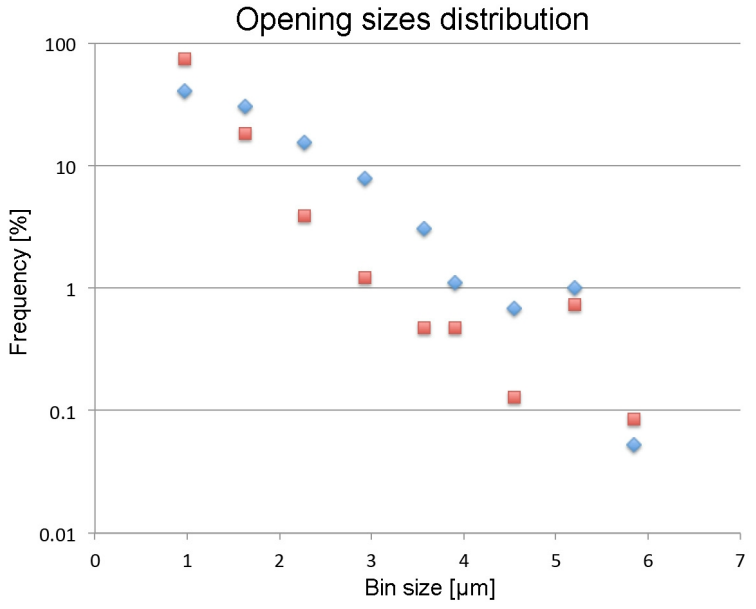
Opening sizes distribution
Frequency [%]
100
10
1
0.1
0.01
0
1
2
3
4
5
6
7
Bin size [µm]

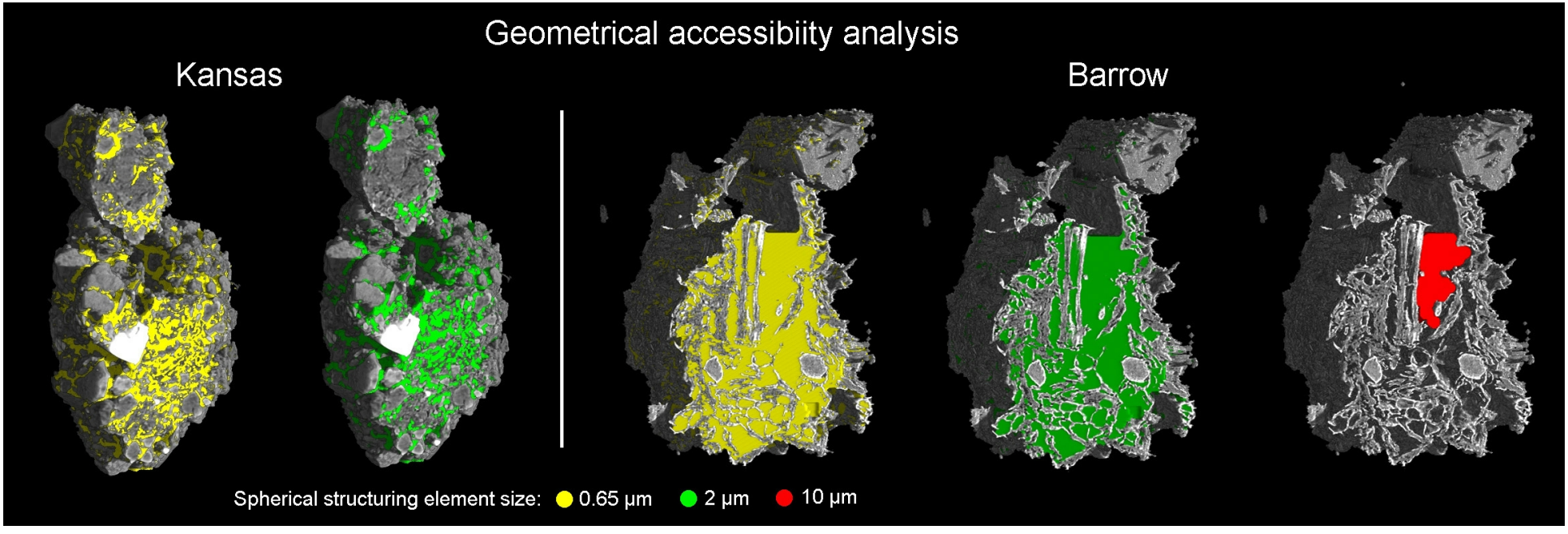
Geometrical accessibiity analysis
Kansas
Barrow
Spherical structuring element size:
0.65 µm
2 µm
10 µm

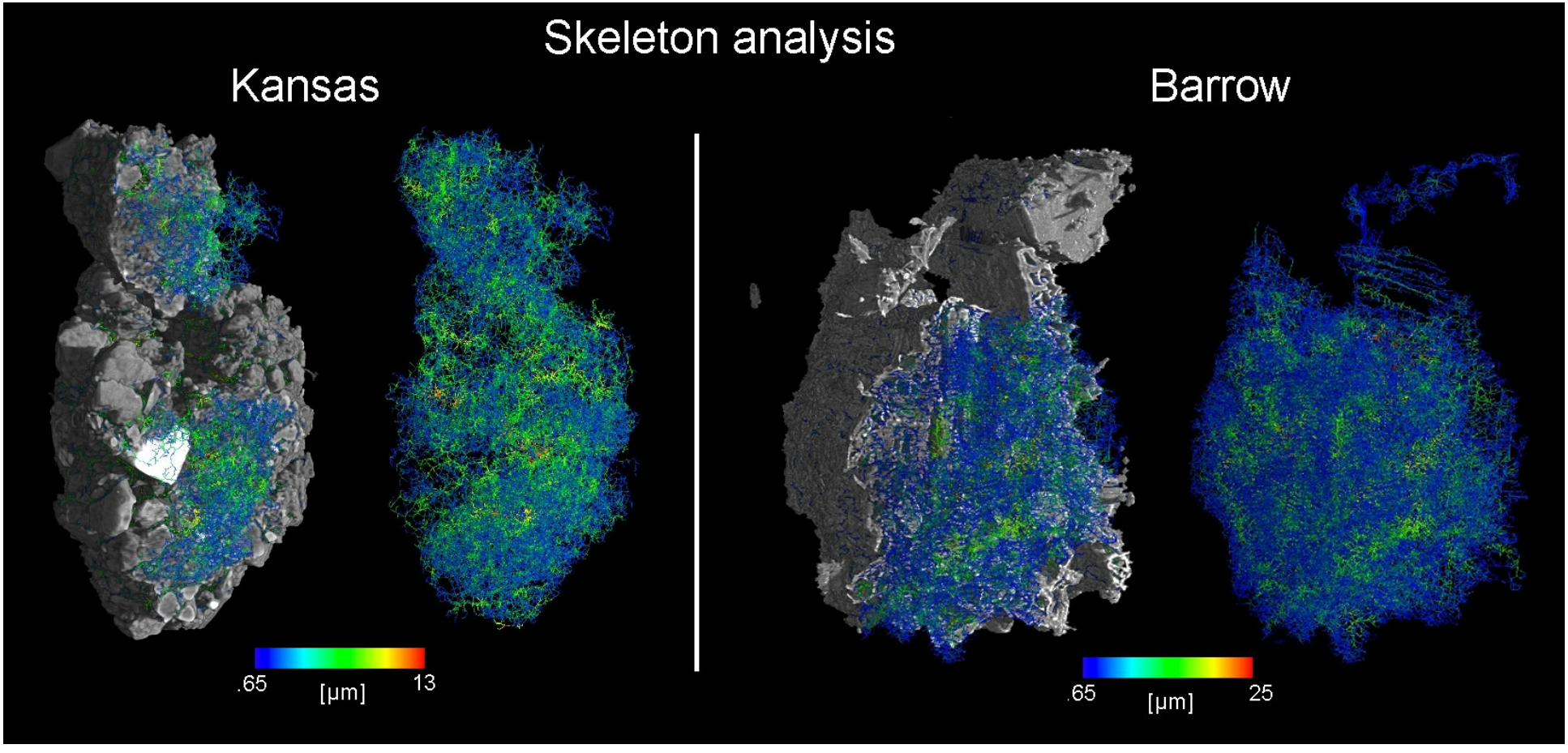
Skeleton analysis
Kansas
Barrow
.65
[µm]
13
.65
[µm]
25

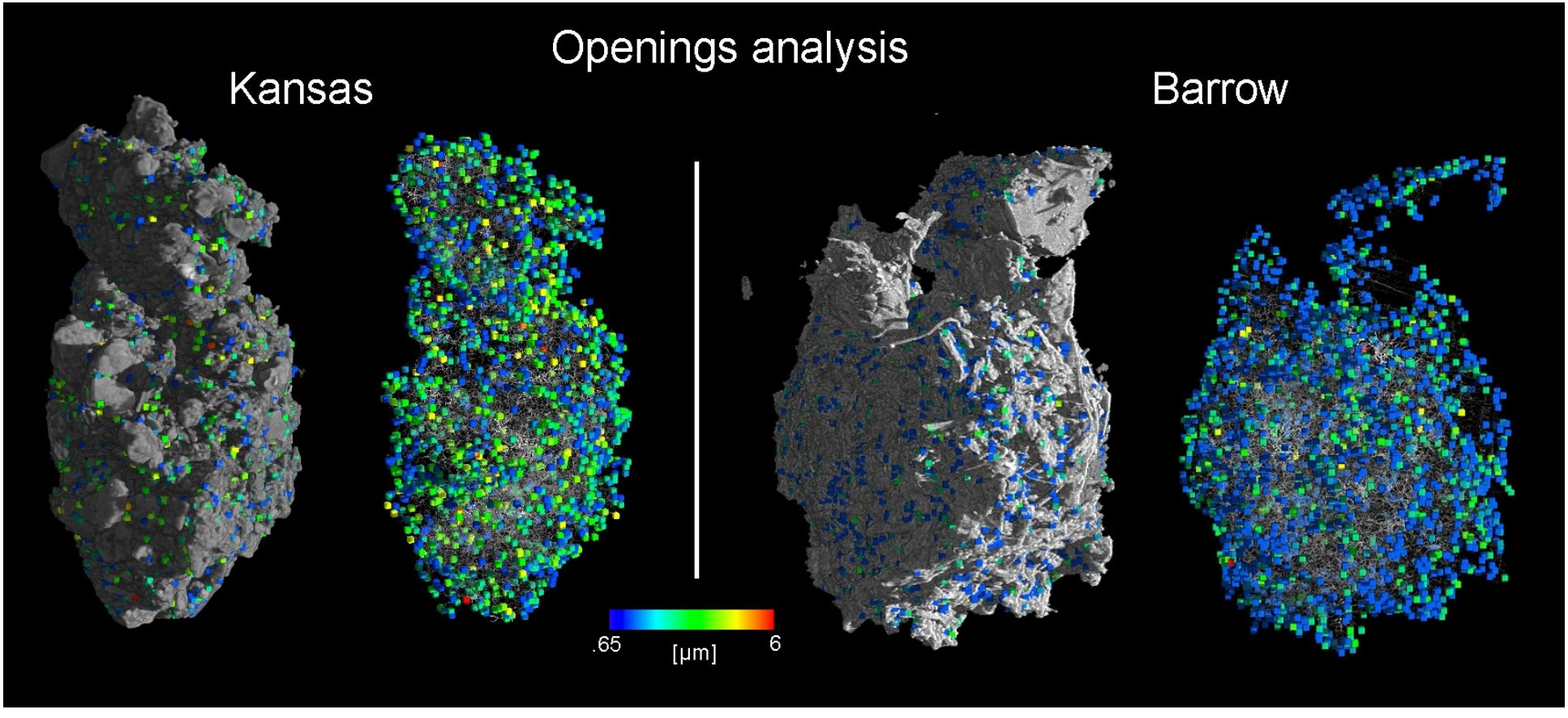
Openings analysis
Kansas
Barrow
.65
[µm]
6

# Anisotropy analysis: Star Length Distributions

## Kansas

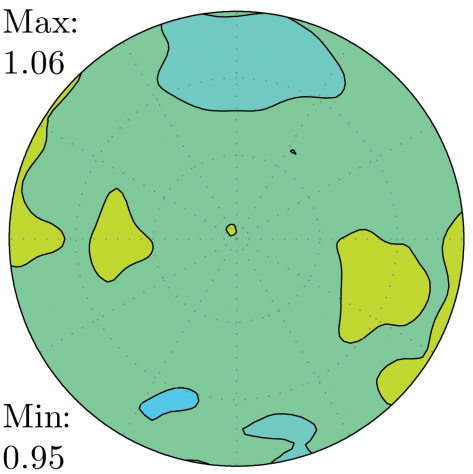


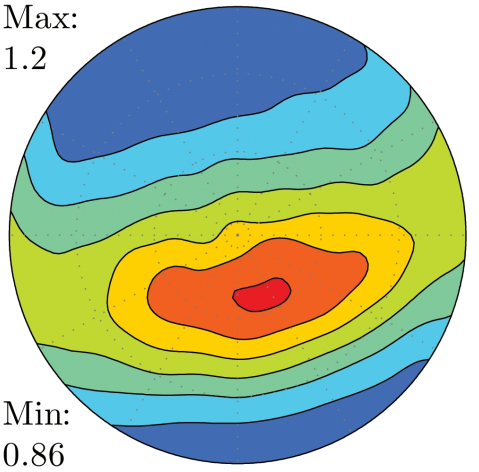


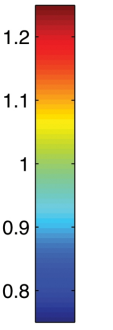


## Barrow

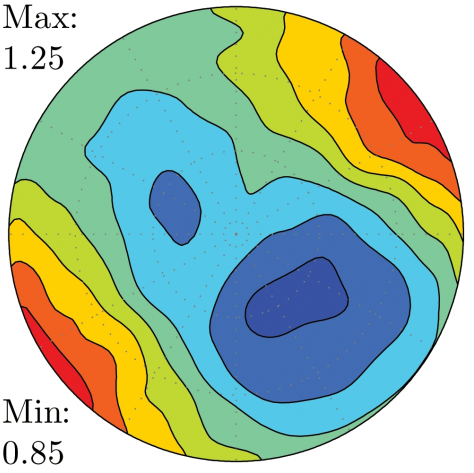


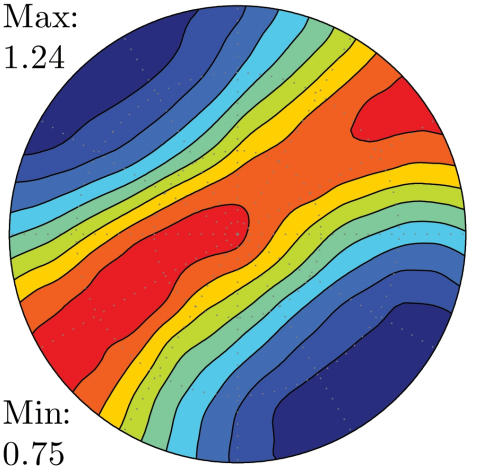


SLD solids

SLD microaggregate shape

Kansas

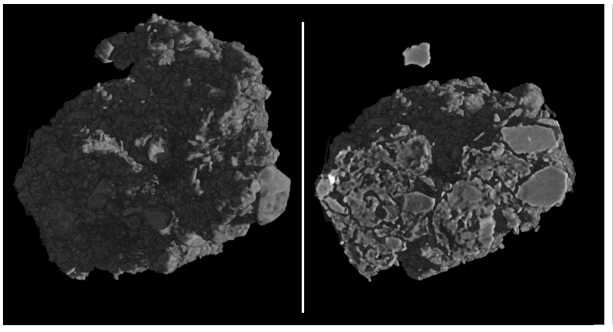

Barrow

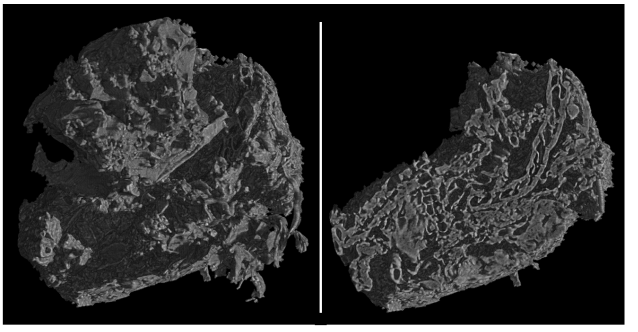

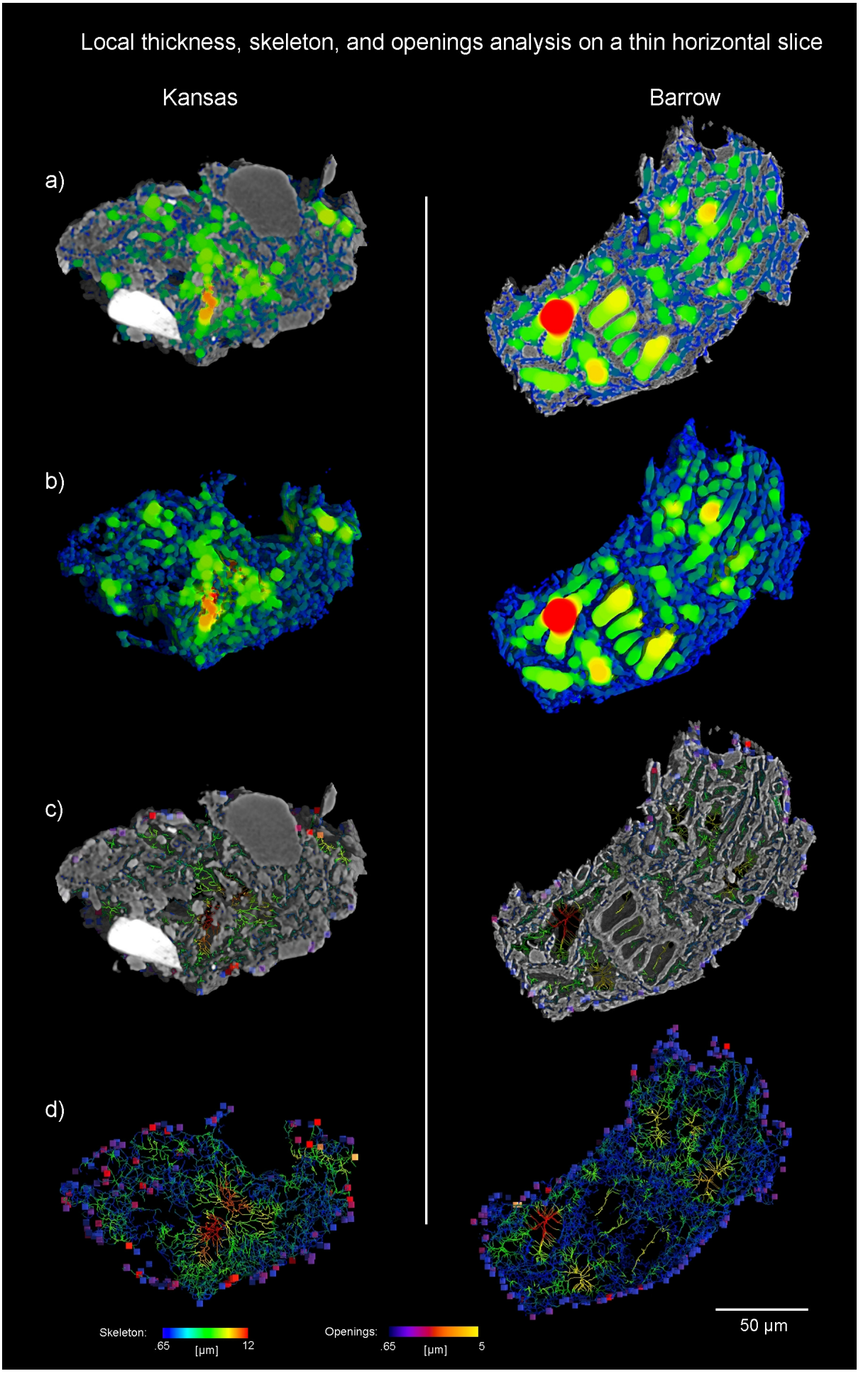
Local thickness, skeleton, and openings analysis on a thin horizontal slice
Kansas
Barrow
a)
b)
c)
d)
Skeleton:
.65
[µm]
12
Openings:
.65
[µm]
5
50 µm